

1 **TITLE PAGE**

- 2
- 3 • **Title:** Computational Model of Cardiovascular Response to Centrifugation and Lower-body
 - 4 Cycling Exercise

5 • **Authors:**

6

- 7 1. Ana Diaz-Artiles¹
- 8 ORCID identifier: orcid.org/0000-0002-0459-9327
- 9 Department of Aerospace Engineering
- 10 Texas A&M University, College Station, TX

11

- 12 2. Thomas Heldt²
- 13 ORCID identifier: orcid.org/0000-0002-2446-1499
- 14 Affiliation:
- 15 Institute for Medical Engineering & Science
- 16 Department of Electrical Engineering & Computer Science
- 17 Massachusetts Institute of Technology, Cambridge, MA.

18

- 19 3. Laurence R. Young²
- 20 Affiliation:
- 21 Department of Aeronautics & Astronautics
- 22 Massachusetts Institute of Technology, Cambridge, MA.

23

- 24 • **Affiliations:**

- 25 • ¹Texas A&M University, College Station, TX
- 26 • ²Massachusetts Institute of Technology, Cambridge, MA

27

- 28 • **Contributions to the study:**

29 Dr. Diaz-Artiles is the main contributor to the article. She implemented the computational

30 model, conducted to human experiments, analyzed the data, prepared figures, and drafted,

31 revised, and approved the final manuscript. Prof. Heldt provided expertise concerning the

32 cardiovascular modeling aspects and interpretation of the experimental data. He also edited,

33 revised, and approved the final version of the manuscript. Prof. Young contributed with the

34 overall supervision and management of the research project, including its relevance to artificial

35 gravity for space travel, and edited, revised, and approved he final version of the manuscript.

- 36
- 37 • **Running Head:** Cardiovascular Model of Centrifugation and Exercise

38

- 39 • **Address for Correspondence:**

40 Ana Diaz Artiles, PhD

41 Texas A&M University, Aerospace Engineering

42 620B H. R. Bright Building

43 Texas A&M University

44 Tel. 979-845-1187

45 adartiles@tamu.edu

48 **ABSTRACT:**

49 Short-radius centrifugation combined with exercise has been suggested as a potential countermeasure
50 against spaceflight deconditioning. Both the long-term and acute physiological responses to such
51 combination are incompletely understood. We developed and validated a computational model to study
52 the acute cardiovascular response to centrifugation combined with lower-body ergometer exercise. The
53 model consisted of 21 compartments, including the upper body, renal, splanchnic, and leg circulation, as
54 well as a four-chamber heart and pulmonary circulation. It also included the effects of gravity gradient
55 and ergometer exercise. Centrifugation and exercise profiles were simulated and compared to
56 experimental data gathered on twelve subjects exposed to a range of gravitational levels (1G and 1.4G
57 measured at the feet) and workload intensities (25-100W). The model was capable of reproducing
58 cardiovascular changes (within ± 1 SD from the group-averaged behavior) due to both centrifugation and
59 exercise, including dynamic responses during transitions between the different phases of the protocol.
60 The model was then used to simulate the hemodynamic response of hypovolemic subjects (blood
61 volume reduced by 5-15%) subjected to similar gravitational stress and exercise profiles, providing
62 insights into the physiological responses of experimental conditions not tested before. Hypovolemic
63 results are in agreement with the limited available data and the expected responses based on
64 physiological principles, although additional experimental data are warranted to further validate our
65 predictions, especially during the exercise phases. The model captures the cardiovascular response for a
66 range of centrifugation and exercise profiles, and it shows promise in simulating additional conditions
67 where data collection is difficult, expensive, or infeasible.

68

69 **KEYWORDS:**

70 Mathematical model, short-radius centrifuge; orthostatic intolerance; cardiovascular simulation; lower
71 body ergometer exercise.

72

73 **NEW & NOTEWORTHY:**

74 Artificial gravity combined with exercise is a potential countermeasure for spaceflight deconditioning,
75 but the long-term and acute cardiovascular response to such gravitational stress is still largely unknown.
76 We provide a novel mathematical model of the cardiovascular system that incorporates gravitational
77 stress generated by centrifugation and lower-body cycling exercise, and we validate it with experimental
78 measurements from human subjects. Simulations of experimental conditions not used for model
79 development corroborate the model's predictive capabilities.

80

81 INTRODUCTION

82 Artificial gravity (AG) generated by centrifugation is a promising countermeasure to mitigate
83 the detrimental effects of weightlessness during space missions (7). Previous ground-based studies have
84 shown that exposure to centrifugation can improve cardiovascular responses to orthostatic stress (18, 35,
85 44, 55), especially if centrifugation is combined with exercise (20, 27–30, 51–53). Artificial gravity has
86 also been proposed as a potential countermeasure to mitigate the recently discovered Spaceflight
87 Associated Neuro-Ocular Syndrome (SANS) (6). Before implementing AG in space, however,
88 additional research efforts are needed to determine the parameters that are most effective, including the
89 angular velocity and radius of the centrifuge, and to characterize the cardiovascular response to these
90 stressors under varying physiological baseline conditions (6). The expensive and time-consuming nature
91 of these experimental studies with human subjects makes the use of computational tools a very
92 attractive approach to systematically study human responses under these conditions.

93
94 Computational cardiovascular models can be used to describe and, more importantly, to predict,
95 human responses in cases where data collection is difficult, expensive, or infeasible. Despite the
96 complexity of the human body, computational approaches of various kinds and anatomical resolution
97 have been successfully applied to a variety of applications, from very detailed three-dimensional models
98 of selected regions, to low-dimensional models representing more aggregate system behavior (i.e.
99 lumped-parameter models). The selection of the type of model is primarily driven by the objectives of
100 the analysis as well as the availability of computational resources (46) and data to specify model
101 parameters and validate the model behavior. In the present work we are interested in the overall, short-
102 term, cardiovascular response to centrifugation combined with exercise and thus, the implementation of
103 a lumped-parameter model seems the appropriate approach.

104
105 One of the first systematic approaches of quantitative, system-level modeling of cardiovascular
106 regulation was developed by Guyton (21, 22). He was one of the first to apply a system engineering
107 approach to quantify and analyze various aspects of cardiovascular function using mathematical and
108 graphical techniques before computers became widely available. Since then, multiple models have been
109 developed to study cardiovascular responses to gravitational stress, including head up tilt (HUT) (25,
110 26, 34), lower-body negative pressure (25, 37), standing-up (15, 38, 39), and centrifugation (54).
111 However, none of these studies have evaluated the effects of centrifugation combined with exercise. The
112 incorporation of the exercise response to the already very complex cardiovascular regulatory
113 mechanisms brings additional physiological and methodological challenges (36) that we attempt to
114 address in our modeling efforts.

115

116 We developed a lumped-parameter model of the cardiovascular system able to capture transient
117 hemodynamic responses to lower-body ergometer exercise under gravitational stress generated by a
118 short-radius centrifuge. The model was built on previous work developed to study short-term
119 hemodynamic responses to centrifugation (54) and exercise (8), but not both mechanisms together at the
120 same time. Our cardiovascular model includes the systemic circulation, four cardiac chambers, and the
121 pulmonary circulation, divided in several parallel branches to account for the gravity gradient associated
122 with short-radius centrifugation. The model also includes the two major short-term neural control
123 mechanisms, the arterial baroreflex and the cardiopulmonary reflex, as well as important exercise
124 mechanisms such as the muscle-pump effect. Experimental measurements collected during a human
125 subject experiment at the Massachusetts Institute of Technology (MIT) short-radius centrifuge were
126 used for validation purposes.

127

128 DESCRIPTION OF THE CARDIOVASCULAR MODEL

129 The cardiovascular system was represented using a lumped-parameter model in which the
130 different vascular segments are represented using electric circuit analogs grouped in compartments.
131 Extensive details of the model architecture and parameters have been published elsewhere (14) and are
132 summarized in the Appendix. A general description of the most relevant features of the model is
133 presented in the following paragraphs.

134

135 The model architecture is shown in **Figure 1**. It contains 21 compartments grouped into four
136 main sections (head and arms, thorax, abdomen, and legs), representing the systemic circulation (15
137 vascular compartments including the arterial system, microcirculation, and the venous system), the
138 cardiac chambers (4 cardiac compartments represented by time-varying elastance models), and the
139 pulmonary circulation (2 additional compartments connected by a microvascular resistance, which we
140 assumed to be linear).

141

142 **Figure 2** shows the architecture of a generic compartment (25, 50). The lumped physical
143 characteristics of each compartment are defined by a resistance R_n and a capacitive element C_n that
144 relates the distending volume $V_{d,n}$ stored in the segment to transmural pressure $\Delta P_n = P_n - P_{ext,n}$. The
145 pressure source $P_{ext,n}$ represents the external pressure acting on the vessels, such as intra-thoracic
146 pressure, intra-abdominal pressure, or muscle-pump pressure. Additionally, the pressure source $P_{h,n}$
147 represents the hydrostatic pressure related to the gravitational orthostatic stress. Other parameters

148 associated with each compartment (not shown in **Figure 2**) include zero-pressure filling volume $V_{0,n}$,
149 and the anatomical vertical length $l_{v,n}$ (superior-to-inferior extension of the vascular segment).

150

151 The flow in each compartment q_n is calculated using the following constitutive relation:

$$q_n = \frac{P_{n-1} - P_n + P_{h,n}}{R_n} \quad (1)$$

152 where P_{n-1}, P_n are the compartment pressures, $P_{h,n}$ is the hydrostatic pressure induced by
153 centrifugation, and R_n is the resistance of the n^{th} compartment.

154

155 The transmural pressure in each compartment, defined as $P_n - P_{ext,n}$, depends on the
156 distending volume $V_{d,n}$, and the compliance of the compartment C_n , through the following linear
157 relationship (except for Compartments 11–splanchnic, 13–leg, and 14–abdominal; see **Figure 1** for
158 compartment numbering scheme):

$$P_n - P_{ext,n} = \frac{V_{d,n}}{C_n} \quad (2)$$

159

160 Some compartments incorporate non-linear elements that affect their behavior. For example, the
161 four cardiac chambers (left atrium, left ventricle, right atrium, right ventricle) are described using time-
162 varying elastance models, and the generation of heartbeats is represented using an Integral Pulse
163 Frequency Modulation (IPFM) model (3, 54). Thus, the contractile force of the myocardial wall is
164 represented by the time-varying capacitors that cycle between a low capacitance (systolic) and a high
165 capacitance (diastolic) state of the myocardium. The intra-thoracic pressure (i.e. external pressure in the
166 thoracic compartments) modulates the filling status of the heart. Further details are included in the
167 Appendix. Moreover, the heart compartments also incorporate unidirectional diodes that represent the
168 cardiac valves and prevent reversal flow. Two vein compartments (Compartments 4–upper body and
169 13–leg) also include diodes to capture the unidirectional nature of the venous flow due to the presence
170 of venous valves.

171

172 Non-linear pressure-volume relationships are also incorporated in some compartments
173 (Compartments 11–splanchnic, 13–leg, and 14–abdominal) to capture their non-linear response when
174 operating at high transmural pressures. In those compartments, the pressure-volume relationship is
175 defined as:

$$V_{t,n} = V_{0,n} + \frac{2V_{max,n}}{\pi} \cdot \arctan\left(\frac{\pi C_{0,n}}{2V_{max,n}} \cdot \Delta P_n\right) \text{ for } \Delta P > 0, \quad n = 11, 13, 14 \quad (3)$$

176 where $V_{t,n}$ denotes the total volume, $V_{0,n}$ denotes the venous unstressed volume or zero-pressure filling
177 volume, $V_{max,n}$ denotes the distending volume limit ($V_{max,11}=1500$ mL, $V_{max,13}=1000$ mL,
178 $V_{max,11}=650$ mL), $C_{0,n}$ denotes the vascular compliance at zero transmural pressure, and ΔP_n denotes
179 the transmural pressure in the n^{th} compartment.

180

181 The cardiovascular model was implemented in MATLAB Simulink. The distending volume is
182 used as the state variable, yielding the following expression for each compartment based on volume
183 conservation principles:

$$\frac{d}{dt}V_{d,n}(t) = q_{in_n} - q_{out_n} \quad (4)$$

184 where q_{in_n} and q_{out_n} correspond to the inward and outward flow in the n^{th} compartment. The complete
185 cardiovascular model is defined by a set of coupled-first order differential equations.

186

187 *Arterial baroreflex and cardiopulmonary control systems*

188 The arterial baroreceptors and the cardiopulmonary receptors are the two major neurally-
189 mediated control systems that ensure short-term cardiovascular regulation in the presence of external
190 disturbances such as orthostatic stress or exercise. They are represented in our model as set-point
191 controllers that serve to minimize an error signal, namely the deviation of a specific local pressure from
192 a pre-defined set-point value, by adjusting various effector mechanisms in a feedback configuration via
193 autonomic pathways. To model the arterial baroreflex, we considered a single lumped baroreceptor in
194 the carotid sinus, assumed to be located 25 cm cranial of the heart. Thus, the carotid sinus pressure, P_{CS} ,
195 is calculated as the aortic arch pressure P_1 minus the hydrostatic column acted upon by short-radius
196 centrifugation. The error signal between the measured pressure and the arterial pressure set-point, P_A^{sp} ,
197 is fed into two linear time-invariant filters (sympathetic and parasympathetic (54)). The resultant signals
198 are then scaled by effector-specific gain values and then applied to the effector variables. The arterial
199 baroreflex effector variables include heart rate, right and left ventricular contractility, and the peripheral
200 resistance and venous unstressed volume of the upper body, renal, splanchnic, and leg compartments.

201

202 The cardiopulmonary reflex is represented using a similar feedback control loop in which the
203 measured variable is the right atrial transmural pressure, ΔP_{RA} , and is compared to the cardiopulmonary
204 set-point pressure, P_{CP}^{sp} . The gains of the sympathetic filter are also specific to each effector variable.
205 The cardiopulmonary reflex effector variables include peripheral resistances and venous unstressed
206 volumes of the upper body, renal, splanchnic, and leg compartments. Both contributions from the

207 arterial baroreflex and the cardiopulmonary reflex constitute the total neurally-mediated global reflex
208 contribution to each effector variable.

209

210 *Centrifugation*

211 We aim to simulate the short-term cardiovascular responses to gravitational stress during short-
212 radius centrifugation. Centrifugation is modeled by: 1) changes in the hydrostatic pressure in all
213 systemic compartments; 2) changes in intrathoracic pressure due to the weight of the liver being pulled
214 in the caudal direction, implemented as changes in the external pressures of the thoracic compartments;
215 and 3) changes in total blood volume due to the increase in transcapillary fluid flow into the dependent
216 vasculature. Short-radius centrifugation induces a gravity gradient along the long body axis in which the
217 hydrostatic pressure depends on the angular velocity and the distance from the center of rotation.
218 Compartments in the lower body are subjected to a higher hydrostatic pressure than compartments in the
219 upper body. The compartmental nature of the model, particularly on the Gz axis, facilitates the
220 representation of these hydrostatic changes along the body's longitudinal axis. Important variables
221 during centrifugation are angular velocity and distances of the CV compartments to the center of
222 rotation (which are dependent of subjects' anthropometry and positioning). The expressions in **Table 1**
223 define the gravitational stress imposed on the individual compartments during gradual exposure to
224 short-radius centrifugation with angular velocity ranging from $\omega = 0$ to $\omega = \omega_{max}$. Additional details
225 of these mathematical expressions and their implementation in the model are included in our previous
226 publications (13, 14).

227

228 *Exercise*

229 Exercise causes circulatory adjustments that are essential to satisfy the metabolic needs of
230 exercising muscles. These adjustments include local vasodilation in exercising muscle groups,
231 sympathetic nervous system activation, an increase in cardiac output, and an increase in arterial blood
232 pressure above the baseline level. In our modeling effort the effects of exercise are represented using the
233 following four mechanisms:

234

235 **Decrease in leg arterial resistance.** Due to the higher metabolic demand during exercise, arterial
236 resistance decreases locally in the exercising muscles to increase local blood flow to satisfy the local
237 metabolic demand, and remove metabolic end products. In our modeling effort, we simulate lower-body
238 cycling exercise by disconnecting the leg resistance from the control systems at the onset of exercise
239 and manually adjusting it to match previously gathered experimental data (10) according to the
240 following expression:

$$R_{lc}(t) = R_{lc}^- + (R_{lf} - R_{lc}^-)(1 - e^{-t/\tau}) \quad (5)$$

241 where R_{lc}^- is the leg vascular resistance immediately before the onset of an exercise phase, R_{lf} is the
 242 final leg vascular resistance for a given exercise intensity, and τ is the time constant governing the
 243 changes in local vascular resistance.

244

245 **Leg muscle pump effect.** During exercise, muscles exert a pump effect by squeezing the veins while
 246 contracting, thus facilitating the return of blood to the heart. In our model, muscle pump effects are
 247 simulated by varying the external pressure at the venous leg compartment periodically, following a
 248 cycling cadence of 1 rev/sec (similar to the subjects' experimental data). The leg external pressure due
 249 to the muscle pump effect, P_{ext}^{pump} , is represented according to:

$$P_{ext}^{pump} = \begin{cases} P_{max}^{pump} \frac{1}{2} (1 - \cos(4\pi t)) & 0 \leq t \leq 1/4 \text{ sec} \\ P_{max}^{pump} & 1/4 \leq t < 1/2 \text{ sec} \\ P_{max}^{pump} \frac{1}{2} (1 + \cos(4\pi(t - 1/2))) & 1/2 \leq t < 3/4 \text{ sec} \\ 0 & 3/4 \leq t < 1 \text{ sec} \end{cases} \quad (6)$$

250 where P_{max}^{pump} is the maximal leg external pressure and depends on the exercise intensity. In addition to
 251 the periodic muscle pump effect during cycling, an external muscle pump pressure P_{spin} , proportional to
 252 the centrifugal force, was added to the venous leg compartment when subjects were not cycling while
 253 they were being centrifuged (i.e. spin-up phase, AG-alone phases, and spin-down phase, see **Figure 3**).
 254 This pressure models the effects of continuous leg muscle activation when subjects are pushed against
 255 the pedals by centrifugal force (similar to the muscle pump caused by "active" standing).

256

257 **Increase in intra-abdominal pressure.** Abdominal pressure increases during exercise due to the
 258 contraction of abdominal muscles. This effect is represented as an increase in external pressure in the
 259 abdominal compartments (7, 8, 9, 10, 11, and 14), according to the following exponential function:

$$P_{ext}^{abd} = P_{max}^{abd} (1 - e^{-t/\hat{\tau}}) \quad (7)$$

260 where $\hat{\tau}$ is a time constant on the order of a few seconds and P_{max}^{abd} is the maximal external pressure that
 261 depends on the intensity of the exercise.

262

263 **Increase in arterial blood pressure.** With increasing exercise intensity, arterial blood pressure
 264 progressively increases over baseline conditions, which cannot be explained on the basis a simple set-
 265 point feedback control system as implemented here. To capture the increased arterial blood pressure, we
 266 made the set-point reference pressure, P_A^{sp} , an adjustable parameter that depends on the exercise
 267 intensity. Thus, P_A^{sp} is considered a tunable parameter to the model. Increases in P_A^{sp} increase

268 sympathetic activity through the arterial baroreceptor control systems previously described. Thus,
269 consequences of increasing the set-point pressure P_A^{SP} include increases in heart rate, ventricular
270 contractility, total peripheral resistance (except in the working muscles), and venous tone.

271

272 *Parameters*

273 Most of the numerical values assigned to the model parameters have been estimated from the
274 literature (24, 25). For each compartment, the parameter assignments include values for resistance R,
275 compliance C, zero-pressure filling volume $V_{0,n}$, and anatomical vertical length $l_{v,n}$. The compartmental
276 parameters and, in addition, the microvascular resistance values, pulmonary and cardiac parameters, as
277 well as parameters related to the control systems are provided in **Table 4** in the Appendix. The
278 parameters related to exercise are specific to our individual simulation profile and are detailed below.

279

280 **SIMULATION PROFILE AND EXPERIMENTAL DATA**

281 We simulated a centrifugation profile identical to the one implemented in a human experiment
282 conducted on the MIT centrifuge (10). The experiment was approved by the Committee on the Use of
283 Humans as Experimental Subjects at MIT. Each subject gave written informed consent to participate in
284 the study. Experimental methods and data analysis are fully described in a previous publication (10). In
285 summary, twelve subjects were positioned in the right-side-down lateral decubitus position with their
286 head positioned at the center of rotation of the MIT centrifuge. The radius of the centrifuge was limited
287 to 1.4m to simulate the space limitations inherent to the short-radius centrifuge proposed for the
288 International Space Station, as part of the “Artificial Gravity with Ergometric Exercise as the
289 Countermeasure for Space Deconditioning in Humans” (AGREE) project (13). Thus, subjects adopted a
290 crouched posture that was taken into account in our simulations by adjusting the leg anatomical vertical
291 lengths l_{v12} and l_{v13} . Subjects were exposed to different levels of centrifugation while performing
292 ergometer exercise at three intensities (25W, 50W, and 100W). The protocol, shown in **Figure 3**,
293 includes the following phases: baseline at rest (3 min), spin-up to the desired G-level (~100 sec), AG
294 phase for subjects to get used to the new gravitational environment (~2 min), the exercise portion of the
295 protocol, which includes three exercise intensities and transitions between them (15 min), another AG
296 phase with no exercise for subjects to partially recover (2 min), and spin-down deceleration phase (1
297 min). The entire protocol was completed in 25 minutes. During the centrifugation runs, continuous,
298 beat-to-beat cardiovascular data were collected using a non-invasive monitoring system (Nexfin
299 monitor, Edwards Lifesciences Corporation, Irvine, CA). Collected variables include heart rate (HR),
300 mean arterial pressure (MAP), systolic blood pressure (SBP), diastolic blood pressure (DBP), pulse
301 pressure (PP), stroke volume (SV), cardiac output (CO), and total peripheral resistance (TPR).

302

303 *Simulation approach*

304 A comparatively small set of physiologically plausible parameters from our model were
305 adjusted to simulate the centrifugation and exercise profiles described above. First, total blood volume
306 was set to $V_{\text{tot}} = 5175$ ml to closely represent our study population. This choice was based on an
307 average of 75 ml of blood per kg of body mass (17, 25, 42) and our experimental subjects' average
308 weight (\pm standard deviation) of 69.3 ± 11.6 kg.

309 Second, the angular velocity, $\omega(t)$, closely replicated the experimental protocol, increasing
310 from 0 rpm to ω_{max} during the spin-up phase, and decreasing back to 0 rpm during the spin-down
311 phase, in both cases following quarter-sine profiles. The experimental AG conditions included 1G and
312 1.4G at the feet, which were the settings of the MIT centrifuge corresponding to a maximum angular
313 velocity of 28.6 and 33.9 rpm, respectively. P_{spin} was also adjusted according to the centrifugation
314 level.

315 Third, the three exercise-related parameters (P_A^{sp} , $P_{\text{max}}^{\text{pump}}$, R_{lf}) were manually adjusted at each
316 workload stage to match the population-averaged MAP and TPR responses (as judged by visual
317 inspections). The decreases in total vascular resistance were simulated by disconnecting the leg
318 peripheral resistance $R_{\text{lc}}(t)$ from the control systems at the onset of exercise, and matching the
319 experimentally observed decreases by appropriately setting the resistance parameters of Eqn. (5). This
320 process was repeated at every workload transition, adjusting the final leg resistance and the time
321 constant to match the experimental data. Similarly, the arterial blood pressure set-point, P_A^{sp} , and the
322 external pressure due to leg muscle pump, $P_{\text{max}}^{\text{pump}}$, were manually adjusted such that the simulated MAP
323 matched the experimental data. The nominal P_A^{sp} was 93 mmHg; it was increased with increasing
324 exercise intensity. The external pressure, $P_{\text{max}}^{\text{pump}}$, was zero at rest and also increased with increasing
325 exercise intensity. Finally, the maximal intra-abdominal pressure, $P_{\text{max}}^{\text{abd}}$, was also increased with
326 increasing exercise intensity in accordance with measurements from the literature (24, 25). For all
327 parameters, transitions between exercise phases were defined by exponential functions with the
328 appropriate time constants to match the experimental data. **Table 2** summarizes all exercise input
329 parameters used in our simulations.

330

331

332 **RESULTS**

333 *Baseline Steady State Simulation*

334 Results during steady-state simulations in supine position show that blood flow and volume
335 distributions to the different vascular beds are within the range of the normal population (47). The
336 distribution of CO to the upper body is 22% (normal range is 15%-29%), 20% to the kidney (18%-
337 24%), 35% to the splanchnic compartment (24%-48%), and 22% to the lower body (14%-33%).
338 Additional details about flow and volume distributions among the compartments are given in **Table 5** in
339 the Appendix.

340

341 *Centrifugation Simulation*

342 **Figure 4** and **Figure 5** show the simulated and experimental cardiovascular responses to
343 centrifugation and ergometer exercise at 1G and 1.4G (measured at the feet), respectively. All major
344 hemodynamic parameters generated by the model stayed within ± 1 SD of the experimental data at
345 almost all times throughout the entire protocol.

346

347 To simulate the exercise protocol, the simulated MAP and TPR responses were matched to the
348 population-averaged experimental responses by adjusting the values of the pressure set-point P_A^{SP} , leg
349 external pressure P_{max}^{pump} , and R_{lc} leg arterial resistance were selected for each exercise level (see **Table**
350 **2**). The top graphs in **Figure 4** and **Figure 5** show that our matching approach captures MAP and TPR
351 very closely. The nominal arterial set-point P_A^{SP} was 93 mmHg, and this value was maintained until the
352 beginning of exercise, when the arterial set-point increased according to the exercise intensity (see
353 **Table 2**). Similarly, during the spin-up phase the simulated TPR responded appropriately to the
354 gravitational stress created by centrifugation: at the beginning of the spin-up phase, the simulated
355 resistance slightly decreased followed by a noticeable increase due to the control system reflexes. This
356 behavior of the TPR is typical of active standing maneuvers (26, 43). At the beginning of the exercise
357 (once the spin-up and AG phases were completed) the leg microvascular resistance was disconnected
358 from the controls and adjusted to decrease such that the simulated TPR matched the experimental data.
359 Thus, the R_{lc} dynamics was composed of three transitions corresponding to the three workload
360 intensities simulated, as shown in the figures.

361

362 The rest of the cardiovascular variables are considered outputs of the simulation. They largely
363 reproduced the general trend of the experiment data, including baseline steady-state conditions as well
364 as the dynamic changes during spin-up/spin-down and exercise transitions. The arterial baroreflex and
365 the cardiopulmonary reflex responded properly to the cardiovascular stress created by centrifugation. In
366 addition, the three exercise phases were very distinguishable from one another, and the time constants
367 during transitions were particularly well matched. During the exercise portion of the protocol, the cyclic

368 muscle pump action is noticeable in most of the simulated cardiovascular variables, making the
369 computational responses oscillate around their mean responses. Thus, during exercise, the simulated
370 responses in **Figure 4** and **Figure 5** manifest themselves as “thicker” lines, due to the periodic external
371 pressure imposed in the venous leg compartment simulating the effects of the cycling exercise
372

373 The simulated heart rate response replicates the experimental data well during all phases of the
374 protocol. Simulated SBP, DBP, SV, and CO are slightly underestimated, especially at higher workloads,
375 though they match the general trends of the data and generally stay within ± 1 SD of the experimental
376 data. The PP simulations reproduce the experimental data for lower work rates (25W and 50W) but
377 underestimate the experimental results for higher work rates (100W). The underestimation of the PP
378 seemed to be driven by the underestimation of systolic pressures, particularly during the intensive
379 exercise phase at 100W (~7% underestimation in both gravitational scenarios), causing the PP
380 underestimation to reach 17% (1G) and 19% (1.4G) at this particular exercise phase. All in all, the
381 systolic, diastolic, and mean ABP were maintained within 10% of experimental values. **Table 3**
382 summarizes the simulated and experimental averages of the CV variables during the different phases of
383 the simulation: baseline, AG alone, exercise at 25W, exercise at 50W, and exercise at 100W. Averages
384 were calculated using the last two minutes of each protocol period, in order to avoid the transient
385 episodes between phases.

386

387 *Case study: Centrifugation of Hypovolemic Subjects due to Microgravity Exposure*

388 Having developed and validated the model for centrifugation and exercise, we can use this
389 model to characterize the cardiovascular response in subjects with specific health conditions, or
390 subjected to new gravitational stress configurations. Additionally, the model can also be used to help
391 test hypotheses about the cardiovascular response in additional scenarios. Physiological reasoning can
392 be used to predict in a qualitative manner specific responses driven by changes in certain parameters.
393 However, the specific magnitude of a response, or degree of impact of particular parameter changes are
394 harder to predict by reasoning alone, given the nonlinear and time-varying nature of the cardiovascular
395 system. As an example, we chose to explore the cardiovascular response to hypovolemic conditions.
396 This scenario is particularly relevant for human spaceflight, since astronauts lose approximately 10% of
397 their blood volume when exposed to extended microgravity (5, 49), which has proven to be problematic
398 when returning to a gravitational environment such as Earth (4, 33), or may become an issue in the
399 future when microgravity adapted individuals are exposed to artificial gravity during spaceflight (12, 19,
400 44, 45). We conducted additional simulations using the same exercise protocol and the centrifugation

401 profile at 1G to investigate cardiovascular responses when blood volume was reduced by 5, 10, and 15%
402 with respect to the euvoletic baseline (nominal $V_{tot}=5175\text{ mL}$).

403

404 Results are shown in **Figure 6** and provide quantitative information about the changes in cardiovascular
405 variables to centrifugation combined with lower-body ergometer exercise. MAP decreases with
406 decreasing levels of blood volume, despite the progressively larger increases in heart rate. The MAP
407 reduction seems to be driven by reduction in SBP, especially during the no-exercise portions of the
408 protocol (BL and AG) where DBP stays relatively constant across all blood volumes tested. PP, SV, and
409 CO also decrease with reducing levels of blood volume. All changes are generally exacerbated at higher
410 work rates, except for HR and TPR, where the responses at 100W across the different blood volume
411 conditions do not differ greatly.

412

413 **DISCUSSION**

414 Several studies have investigated the short-term hemodynamics response of exercise in the
415 upright and supine posture (1, 11), and as a potential countermeasure in ground-based bedrest studies
416 (40). Our focus here is on the acute cardiovascular response to a gravitational stress that can be
417 recreated in space and that is not constant along the major body axis. We developed a lumped-parameter
418 model of the cardiovascular system to simulate the short-term hemodynamic responses to combined
419 gravitational stress and exercise. In particular, gravitational stress was generated by centrifugation of
420 subjects using a short-radius centrifuge, therefore generating a high gravity gradient along the long axis
421 of the body. The model simulates the hydrostatic pressures among cardiovascular compartments caused
422 by the gravity gradient. In addition, the effects of ergometer exercise were also incorporated in the
423 model, including the increase in blood pressure, the muscle pump effect, the decrease in vascular
424 resistance, and changes in intra-abdominal pressure. Finally, the model was programmed to recreate the
425 25-min exercise protocol experienced by 12 subjects in a previous human experiment conducted at MIT
426 (10). Although there have been other studies investigating centrifugation combined with ergometer
427 exercise (16, 27–29, 45, 48, 51), these studies have mainly focused on physiological responses *before*
428 and *after* a specific intervention (e.g. bed rest or training protocol) and not *during* the centrifugation
429 sessions. Thus, the cardiovascular data taken during the MIT centrifugation experiments were used to
430 calibrate and evaluate the computational model. Thus, we are combining mathematical modeling and
431 human experiments in a synergistic manner. On the one hand, experiments are necessary for specifying
432 model parameters and for model validation; on the other hand, models allow for flexibility to investigate
433 physiological mechanisms under consideration, enhance experimental data interpretation, and serve as a
434 vehicle to test competing hypothesis.

435

436 Generally, the cardiovascular model matched the dynamic cardiovascular response during the
437 25-min exercise protocol quite well. It showed a slight tendency to underestimate some of the
438 cardiovascular variables, particularly SV, and PP at higher workload intensities, and to a lesser extent,
439 CO. These results could be better adjusted by modifying some of the numerous parameters that are built
440 in the model. However, it is important to emphasize that the purpose of these simulations is to
441 intentionally limit the number of inputs and not to exert the full flexibility of the model to reduce the
442 error between the experimental and simulated responses. A small number of parameters, namely TPR
443 and MBP, have been constrained to determine if the resulting simulations capture the physiologic
444 response over a range of exercise levels and AG regimes. The multi-compartment model has more than
445 100 parameters and it can be manipulated to perfectly match the cardiovascular responses. However, the
446 value of such an exercise is small, as most parameters will have negligible influence on the output and
447 the resultant solution will therefore not be unique and will not provide much physiological insights.

448

449 Overall, the cardiovascular model developed in this research effort provides unique information
450 about the cardiovascular responses to gravitational stress and exercise. Model results and comparisons
451 during the baseline period are particularly interesting since they provide a good indication of the
452 cardiovascular modeling performance without any stressor such as centrifugation or exercise. A finite
453 number of hemodynamic compartments and the primary exercise mechanisms were included in the
454 model. Although we recognize that exercise is a particularly complex activity from the physiological
455 modeling point of view, our results show that our model included enough vascular and exercise
456 mechanisms to attain suitable accuracy, at least within the selected ranges of AG and exercise intensity.
457 As Reisner and Heldt pointed out (41), this refers to the “immortal problem of modeling”: creating a
458 model simple enough to feasibly determine the outputs with enough accuracy, without including
459 superfluous complexity that can make difficult the fundamental understanding of the model (i.e. how
460 individual parts interact with each other).

461

462 To explore the physiological consequences of centrifugation we further studied quantitative
463 responses to centrifugation and exercise in hypovolemic subjects, with reduction of 5, 10, and 15% of
464 total blood volume. There is limited experimental data in the literature to perform a direct comparison
465 between our simulations and hemodynamic responses from hypovolemic subjects subjected to short-
466 radius centrifugation an exercise. Thus, we base our comparison to a similar study that used tilt tests
467 maneuvers to study orthostatic stress. Linnarsson and his colleagues (35) investigated orthostatic
468 tolerance in hypovolemic subjects after five days of bedrest. Subjects lost between 8-14% of blood

469 volume during the 5-day bed rest, and their short-term, post-bedrest HR, SYS, and DIA responses
470 during a tilt test (80° upright) changed approximately +29%, -15%, and -5% respectively, with respect
471 to pre-bed rest. Our data indicate that hypovolemic subjects presenting blood volume losses between 10-
472 15% will also experience increases in HR (+14 to 17%) and decreases in SYS (-10.5 to -15.6%) and
473 DIA (-2.8 to -5.7%). We expect to see less significant changes in a short-radius centrifuge due to the
474 presence of a strong gravity gradient that makes the gravitational stress less intense than being exposed
475 to constant 1G gravitational environment. Thus, our simulations seem to be in agreement with the
476 limited available data and the expected responses based on physiological principles. Additional
477 experiments are warranted to further validate the predicted values from our model, particularly the ones
478 involving exercise. However, these predictions are already providing insightful information about
479 experimental conditions not tested before.

480

481 *Limitations*

482 We chose to represent the cardiovascular behavior using a lumped-parameter model. This
483 approach is unable to simulate pulse wave propagation phenomena such as the changes in arterial
484 pressure waveform as it propagates through the arterial system (31, 50) and might therefore be
485 responsible for our underestimation of systolic blood pressure at higher centrifugation level and exercise
486 regimes. Despite this limitation our model was able to reproduce realistic responses at a lower
487 computational cost. Inertial effects were also not included in the model causing, for example, the
488 absence of the dichrotic notch typically present in the arterial and pulmonary arterial waveforms during
489 closure of the semilunar valves. Inertial effects become important when studying intra-beat changes
490 (within a cardiac cycle), which is not the case in the present study. Inertial effects have been estimated
491 to account for less than 1% of stroke volume and mean arterial pressure (9) and therefore they have been
492 neglected.

493 We have also not taken into account possible non-linear cardiac effects. Both systolic and
494 diastolic pressure-volume relationships were assumed to be linear, which is reasonable at normal filling
495 pressures, but these relationships become non-linear at higher filling pressures. Simulations of
496 pathologically high pressures were beyond of the scope of this work, and for the purpose of the
497 simulations presented here, the pressure-volume relationships were assumed linear. Additionally, the
498 unstressed volume was assumed to be static throughout the cardiac cycle and the same for the diastolic
499 and systolic pressure-volume relationships. Typically, the end-systolic unstressed volume is between
500 25-40% lower than its diastolic counterpart (2, 32), indicating a small but potentially significant
501 contribution to stroke volume, thus decreasing the underestimation seen in our simulations.

502 Viscoelastic stress-relaxation effects of the systemic veins were also not included in our
503 modeling effort. This phenomenon refers to the intrinsic ability of the vascular walls to stretch slowly
504 when the pressure rises and to contract slowly when the pressure falls (23, 26). This effect becomes
505 important when studying very short-term (~30 s) dynamic blood pressure responses after exposure to
506 passive head-up tilt, due to the altering of the time-course of venous pooling to the lower body and thus,
507 limiting the blood pressure dip typically seen during active standing (26). In our work we focused on
508 steady-state cardiovascular responses during active exposure to centrifugation and therefore these
509 effects were also neglected. We have also not taken into account breathing-related changes in
510 intrathoracic pressure. As the depth of breathing increases with increasing exercise, the lowering of
511 intrathoracic pressure aids in venous return at higher exercise levels. We have also assumed that the
512 resistance changes due to exercise are largely determined by the arteriolar vasodilation and that the
513 muscle pump primarily affects the filling state of the leg veins.

514 Finally, we have already commented on the difficulty of assigning numerical values to all the
515 parameters of the model. The degree to which our model reproduces the experimental data suggests that
516 we have included all the major features with a reasonable degree of parameter accuracy. Sensitivity
517 analysis techniques could elucidate the influence of each parameter on the model outputs to determine
518 the subset of physiological parameters that dominate the model response. This could be further related
519 to individual differences seen in hemodynamic responses to gravitational stress across specific
520 population, such as astronauts coming back to Earth after being exposed to microgravity conditions.

521

522 *Conclusion*

523 We have developed a computational model of the cardiovascular system capable of reproducing
524 hemodynamic responses during gravitational stress generated by a short-radius centrifuge and lower-
525 body ergometer exercise. The model simulated both transient and steady-state responses that compare
526 well with experimental data gathered on twelve subjects that underwent the same simulated protocol
527 using the MIT short-radius centrifuge. We explored the capabilities of the model to generate new
528 hypotheses and to quantify changes in cardiovascular responses due to variations in an individual
529 parameter (i.e. total blood volume).

530

531 **APPENDIX**

532 **A. Additional Details about the Cardiovascular Model**

533 Most of the model equations have already been reported in a previous publication (14), but for
 534 completeness, we are including them in this Appendix.

535

536 *Cardiac Model*

537 The four cardiac chambers are simulated using time-varying elastance models (24, 25). The
 538 time-varying elastance in each one of the four cardiac chambers is represented using the equation below,
 539 where the time interval of diastolic relaxation T_d^r is assumed to be one half of the systolic time interval
 540 T_s :

$$E(t) = \begin{cases} E_d + \frac{E_{es} - E_d}{2} \cdot \left\{1 - \cos\left(\pi \frac{t}{T_s}\right)\right\} & 0 \leq t \leq T_s \\ E_d + \frac{E_{es} - E_d}{2} \cdot \left\{1 + \cos\left(2\pi \frac{t}{T_s}\right)\right\} & T_s < t \leq \frac{3}{2}T_s \\ E_d & \frac{3}{2}T_s < t \end{cases} \quad (8)$$

541 and E_d and E_{es} are the diastolic elastance and end-systolic elastances in each one of the four cardiac
 542 chambers, respectively. The timing parameters include the atrial and ventricular systole duration, T_s^a
 543 and T_s^v , as well as the ‘‘P-R interval’’, which we defined here as the delay between the onset of the atrial
 544 and ventricular contraction T_{a-v} . Their values are assumed to be proportional to the square root of the
 545 R-R interval length T_{RR} (24, 25) and are defined as $T_s^a(s) = 0.2\sqrt{T_{RR}}$, $T_s^v(s) = 0.3\sqrt{T_{RR}}$, and
 546 $T_{a-v}(s) = 0.12\sqrt{T_{RR}}$

547

548 The cardiac pacemaker is represented using an Integral Pulse Frequency Modulation (IPFM)
 549 model (3, 24, 25, 54), according to:

$$M(t) = \int_{t_{k-1}}^t m(t)dt = \int_{t_{k-1}}^t (m_0 + m_r(t))dt$$

550 where $M(t)$ mimics the behavior of the transmembrane potential in the sino-atrial node whose value at
 551 time t depends on the cumulative automaticity m_0 (assumed constant), and the contribution of neural
 552 control input $m_r(t)$ (either sympathetic or parasympathetic activity) since the end of the last heartbeat
 553 (or cardiac excitation time $t_k - 1$). A new heartbeat occurs at the time t_k when the transmembrane
 554 potential $M(t)$ reaches a predefined threshold potential $\Gamma = 1$, and the time since the previous heartbeat
 555 is at least one fifth of the preceding cardiac cycle length:

556
$$\int_{t_{k-1}}^{t_k} m(t)dt = M(t_k) \geq \Gamma \quad \text{and} \quad t_k - t_{k-1} \geq 0.2(t_{k-1} - t_{k-2})$$

557
558
559

The function $m(t)$ is defined as the inverse of the instantaneous R-R interval $I(t)$:

$$m(t) = \frac{1}{I(t)} = \frac{1}{I_0 + \Delta I_{AB}(t)}$$

560 where I_0 is the nominal R-R interval, and $\Delta I_{AB}(t)$ is the control input from the arterial baroreflex
561 control system.

562

563 *Control Systems*

564 The baroreceptor control system is modeled using a negative feedback loop and an arterial
565 pressure set-point P_A^{sp} . Assuming one lumped baroreceptor located in the carotid sinus at 25 cm above
566 the heart, the carotid sinus pressure P_{CS} (mmHg) is defined as:

$$P_{CS} = P_1 - \frac{1}{2} \cdot \rho \cdot \omega^2(t) \cdot ((25 + d)^2 - d^2) \quad (9)$$

567 where d is the distance between the head and the center of rotation measured in cm, ρ is the blood
568 density in $\frac{mmHg}{1/s^2 cm^2}$, and $\omega(t)$ is the angular velocity of the centrifuge in rad/s. The feedback error signal

569 $e_{AB}(t)$ is calculated as follows:

$$e_{AB}(t) = 18 \cdot \arctan\left(\frac{P_{CS} - P_A^{sp}}{18}\right) \quad (10)$$

570

571 The cardiopulmonary reflex is also modeled using a negative feedback loop and a pressure set-
572 point P_{CP}^{sp} . The variable measured is the transmural right atrial pressure ΔP_{RA} and the error signal
573 $e_{CP}(t)$ is calculated as follows:

$$e_{CP}(t) = 5 \cdot \arctan\left(\frac{\Delta P_{RA} - P_{CP}^{sp}}{5}\right) \quad (11)$$

574

575 The sympathetic and parasympathetic control systems are modeled as two linear time-invariant
576 (LTI) filters. The transfer functions for the sympathetic $s(s)$ and parasympathetic $p(s)$ filters are:

$$s(s) = \frac{1}{42s^2} e^{-2s} + \frac{1}{75s^2} e^{-5s} + \frac{1}{300s^2} e^{-30s} \quad (12)$$

577

$$p(s) = 1 \quad (13)$$

578

579 *Transcapillary Flow and the Interstitial Fluid Volume*

580 Orthostatic stress causes a decrease in intravascular volume due to an increase in transcapillary
 581 fluid flow to the dependent vasculature. This phenomenon can be represented using additional RC
 582 compartments (24, 25, 54). The transcapillary flow is solved analytically based on the orthostatic stress
 583 profile using the equations described in the following section. The solution of the equations depends on
 584 two parameters: the time constant $\tau = RC = 4.6 \text{ min}$ (24, 25), and the maximum interstitial volume
 585 change $V_{max} = P_h C$, given in **Table 1**. The transcapillary flow is then subtracted from the venous return
 586 at the selected compartments where this phenomenon is significant: splanchnic venous (compartment
 587 11), leg venous (compartment 13), and abdominal venous (compartment 14). The fractions of interstitial
 588 volume and interstitial flow assigned to each compartment are defined below:

$$V^n(t) = \frac{P_{h,max}^n}{\sum_i P_{h,max}^i} \cdot V(t) \quad (14)$$

589

$$q^n(t) = \frac{P_{h,max}^n}{\sum_i P_{h,max}^i} \cdot q(t) \quad (15)$$

590

591 where $P_{h,max}^n$ is the maximum hydrostatic pressure in the n^{th} compartment; and $\sum_i P_{h,max}^i$ is the sum of
 592 the maximum hydrostatic pressures of the three compartments (11, 13, and 14).

593

594 *Analytical Solutions for the Transcapillary Flow and the Interstitial Fluid Volume*

595 The following equations provide an analytical solution for the intercapillary flow and interstitial
 596 volume change during gravitational stress.

597

598 Region I: Gradual increase in orthostatic stress over a period of length Δt .

$$q(t) = \frac{V_{max}}{\Delta t} \cdot (1 - e^{-\frac{t}{\tau}}) \quad (16)$$

$$V(t) = V_{max} \cdot \left(\frac{t}{\Delta t} - \frac{\tau}{\Delta t} \left(1 - e^{-\frac{t}{\tau}} \right) \right) \quad (17)$$

599 Region II: Full gravitational stress during period of duration T_{tilt} .

$$q(t) = \frac{V_{max}}{\Delta t} \cdot (1 - e^{-\frac{\Delta t}{\tau}}) \cdot e^{-\frac{t-\Delta t}{\tau}} \quad (18)$$

$$V(t) = V_{max} \cdot \left(1 - \frac{\tau}{\Delta t} \left(1 - e^{-\frac{\Delta t}{\tau}} \right) e^{-\frac{t-\Delta t}{\tau}} \right) \quad (19)$$

600 Region III: Gradual decline in gravitational stress over a period of length Δt .

$$q(t) = \frac{V_{max}}{\Delta t} \cdot \left(1 + \left(1 - e^{-\frac{\Delta t}{\tau}} \right) e^{-\frac{T_{tilt}}{\tau}} \right) \cdot e^{-\frac{t-(\Delta t+T_{tilt})}{\tau}} - \frac{V_{max}}{\Delta t} \quad (20)$$

$$V(t) = V_{max} \cdot \left(1 - \frac{t - (\Delta t + T_{tilt})}{\Delta t}\right) - V_{max} \cdot \frac{\tau}{\Delta t} \cdot \left(1 - e^{-\frac{\Delta t}{\tau}}\right) \cdot e^{-\frac{T_{tilt}}{\tau}} + \quad (21)$$

$$+ V_{max} \cdot \frac{\tau}{\Delta t} \cdot \left(1 + \left(1 - e^{-\frac{\Delta t}{\tau}}\right) e^{-\frac{T_{tilt}}{\tau}}\right) \cdot \left(1 - e^{-\frac{t - (\Delta t + T_{tilt})}{\Delta t}}\right)$$

601 Region IV: Post-orthostatic stress recovery of unspecified length.

$$q(t) = -\frac{V_{max}}{\Delta t} \cdot \left(1 - e^{-\frac{\Delta t}{\tau}}\right) \cdot \left(1 - e^{-\frac{T_{tilt} + \Delta t}{\tau}}\right) \cdot e^{-\frac{t - (2\Delta t + T_{tilt})}{\tau}} \quad (22)$$

$$V(t) = V_{max} \cdot \frac{\tau}{\Delta t} \cdot \left(1 - e^{-\frac{\Delta t}{\tau}}\right) \cdot \left(1 - e^{-\frac{T_{tilt} + \Delta t}{\tau}}\right) \cdot e^{-\frac{t - (2\Delta t + T_{tilt})}{\tau}} \quad (23)$$

602

603 *Initial Conditions*

604 The following 23 non-linear algebraic equations are used to find the initial conditions, and they
 605 describe the blood flow in the compartments assuming that the system is in steady state (54). The first
 606 equation equates the right ventricular stroke volume and the left ventricular stroke volume, and the last
 607 equation is based on the conservation of volume equating the difference between the total volume and
 608 the unstressed volume, and the distending volume in each compartment.

609

$$C_{ld}(P_{lvd} - P_{th}) - C_{ls}(P_{lvs} - P_{th}) = C_{rd}(P_{rvd} - P_{th}) - C_{rs}(P_{rvs} - P_{th}) \quad (24)$$

$$C_{ld}(P_{lvd} - P_{th}) - C_{ls}(P_{lvs} - P_{th}) = T_s^v \cdot \frac{P_{lvd}}{R_1} \quad (25)$$

$$T_s^v \cdot \frac{P_{lvd}}{R_1} = I_0 \cdot \left(\frac{P_1 - P_2}{R_2} + \frac{P_1 - P_6}{R_6}\right) \quad (26)$$

$$I_0 \cdot \frac{P_1 - P_2}{R_2} = I_0 \cdot \frac{P_2 - P_3}{R_3} \quad (27)$$

$$I_0 \cdot \frac{P_2 - P_3}{R_3} = I_0 \cdot \frac{P_3 - P_4}{R_{ub}} \quad (28)$$

$$I_0 \cdot \frac{P_3 - P_4}{R_{ub}} = I_0 \cdot \frac{P_4 - P_5}{R_4} \quad (29)$$

$$I_0 \cdot \frac{P_4 - P_5}{R_4} = I_0 \cdot \frac{P_5 - P_{ra}}{R_5} \quad (30)$$

$$I_0 \cdot \frac{P_1 - P_6}{R_6} = I_0 \cdot \frac{P_6 - P_7}{R_7} \quad (31)$$

$$I_0 \cdot \frac{P_6 - P_7}{R_7} = I_0 \cdot \left(\frac{P_7 - P_8}{R_8} + \frac{P_7 - P_{10}}{R_{10}} + \frac{P_7 - P_{12}}{R_{12}}\right) \quad (32)$$

$$I_0 \cdot \frac{P_7 - P_8}{R_8} = I_0 \cdot \frac{P_8 - P_9}{R_{rc}} \quad (33)$$

$$I_0 \cdot \frac{P_8 - P_9}{R_{rc}} = I_0 \cdot \frac{P_9 - P_{14}}{R_9} \quad (34)$$

$$I_0 \cdot \frac{P_7 - P_{10}}{R_{10}} = I_0 \cdot \frac{P_{10} - P_{11}}{R_{sc}} \quad (35)$$

$$I_0 \cdot \frac{P_{10} - P_{11}}{R_{sc}} = I_0 \cdot \frac{P_{11} - P_{14}}{R_{11}} \quad (36)$$

$$I_0 \cdot \frac{P_7 - P_{12}}{R_{12}} = I_0 \cdot \frac{P_{12} - P_{13}}{R_{lc}} \quad (37)$$

$$I_0 \cdot \frac{P_{12} - P_{13}}{R_{lc}} = I_0 \cdot \frac{P_{13} - P_{14}}{R_{13}} \quad (38)$$

$$I_0 \cdot \frac{P_{14} - P_{15}}{R_{14}} = I_0 \cdot \left(\frac{P_9 - P_{14}}{R_9} + \frac{P_{11} - P_{14}}{R_{11}} + \frac{P_{13} - P_{14}}{R_{13}} \right) \quad (39)$$

$$I_0 \cdot \frac{P_{14} - P_{15}}{R_{14}} = I_0 \cdot \frac{P_{15} - P_{ra}}{R_{15}} \quad (40)$$

$$I_0 \cdot \left(\frac{P_5 - P_{ra}}{R_5} + \frac{P_{15} - P_{ra}}{R_{15}} \right) = T_d^v \cdot \frac{P_{ra} - P_{rvd}}{R_{tri}} \quad (41)$$

$$T_d^v \cdot \frac{P_{ra} - P_{rvd}}{R_{tri}} = T_s^v \cdot \frac{P_{rvd} - P_{pa}}{R_{ro}} \quad (42)$$

$$T_s^v \cdot \frac{P_{rvd} - P_{pa}}{R_{ro}} = I_0 \cdot \frac{P_{pa} - P_{pv}}{R_{pv}} \quad (43)$$

$$I_0 \cdot \frac{P_{pa} - P_{pv}}{R_{pv}} = I_0 \cdot \frac{P_{pv} - P_{la}}{R_{li}} \quad (44)$$

$$I_0 \cdot \frac{P_{pv} - P_{la}}{R_{li}} = T_d^v \cdot \frac{P_{la} - P_{lvd}}{R_{mit}} \quad (45)$$

$$V_{total} - V_{total}^0 = \sum_{j \in \left\{ \begin{array}{l} 1,2,\dots,10, \\ 12,15,ra,rv, \\ pa,pv,la,lv \end{array} \right\}} C_j \cdot \Delta P_j + \sum_{k \in \{11,13,14\}} \left[\frac{2V_{maxk}}{\pi} \cdot \arctan \left(\frac{\pi C_{0k}}{2V_{maxk}} \cdot \Delta P_k \right) \right] \quad (46)$$

610

611

612

613 B. Parameters of the Cardiovascular Model

614

615 (Insert Table 4)

616

617 C. Baseline Steady State Flows and Volume Distributions

618

619

(Insert Table 5)

620

621

622 **ACKNOWLEDEMENTS**

623 We thank the subjects who kindly participated in the experimental study conducted at the
624 Massachusetts Institute of Technology.

625

626 **GRANTS**

627 This project was supported by the MIT/Skolkovo development project (Seed Grant 6925991),
628 and the National Space Biomedical Research Institute through NASA NCC 9-58. In addition, the
629 Fulbright Commission has provided additional support.

630

631 **DISCLOSURES**

632 No conflicts of interest, financial or otherwise, are declared by the authors.

633

634

635

636 REFERENCES

- 637 1. **Ade CJ, Broxterman RM, Barstow TJ.** Effects of body posture and exercise training on
638 cardiorespiratory responses to exercise. *Respir Physiol Neurobiol* 188: 39–48, 2013.
- 639 2. **Alexander J, Sunagawa K, Chang N, Sagawa K.** Instantaneous pressure-volume relation of
640 the ejecting canine left atrium. *Circ Res* 61: 209–219, 1987.
- 641 3. **de Boer RW, Karemaker JM, Stracke J.** Description of the Heart_Rate Variability Data in
642 Accordance With a Physiological Model for the Genesis of Heartbeats. *Psychophysiology* 22:
643 147–155, 1985.
- 644 4. **Buckey JC, Lane LD, Levine BD, Watenpaugh DE, Wright SJ, Moore WE, Gaffney FA,
645 Blomqvist CG.** Orthostatic intolerance after spaceflight. *J Appl Physiol* 81: 7–18, 1996.
- 646 5. **Charles BJ, Lathers CM.** Cardiovascular Adaption to Spaceflight. *J Clin Pharmacol* 31: 1010–
647 1023, 1991.
- 648 6. **Clément G.** International roadmap for artificial gravity research. *npj Microgravity* 3: 29, 2017.
- 649 7. **Clement GR, Bukley AP, Paloski WH.** Artificial gravity as a countermeasure for mitigating
650 physiological deconditioning during long-duration space missions. *Front Syst Neurosci* 9: 92,
651 2015.
- 652 8. **Croston RC, Rummel J a., Kay FJ.** Computer model of cardiovascular control system
653 responses to exercise. *J. Dyn. Syst. Meas. Control* (1973). doi: 10.1115/1.3426719.
- 654 9. **Defares JG, Osborn JJ, Hara HH.** Theoretical synthesis of the cardiovascular system. Study I:
655 The controlled system. *Acta Physiol Pharmacol Neerl* 12: 189–265, 1963.
- 656 10. **Diaz-Artiles A, Heldt T, Young LR.** Short-Term Cardiovascular Response to Short-Radius
657 Centrifugation With and Without Ergometer Exercise. *Front Physiol* 9: 1492, 2018.
- 658 11. **Diaz-Artiles A, Navarro Tichell P, Perez F.** Cardiopulmonary Responses to Sub-Maximal
659 Ergometer Exercise in a Hypo-Gravity Analog Using Head-Down Tilt and Head-Up Tilt. *Front*
660 *Physiol* 10: 1–15, 2019.
- 661 12. **Diaz A, Heldt T, Young LR.** Cardiovascular responses to artificial gravity combined with
662 exercise. In: *2015 IEEE Aerospace Conference Proceedings*. Big Sky, MT: 2015.
- 663 13. **Diaz A, Trigg C, Young LR.** Combining ergometer exercise and artificial gravity in a compact-
664 radius centrifuge. *Acta Astronaut* 113: 80–88, 2015.
- 665 14. **Diaz Artiles A, Heldt T, Young LR.** Effects of artificial gravity on the cardiovascular system:
666 Computational approach. *Acta Astronaut* 126: 395–410, 2016.
- 667 15. **Ellwein LM, Tran HT, Zapata C, Novak V, Olufsen MS.** Sensitivity Analysis and Model
668 Assessment: Mathematical Models for Arterial Blood Flow and Blood Pressure. *Cardiovasc Eng*
669 8: 94–108, 2008.
- 670 16. **Evans JM, Stenger MB, Moore FB, Hinghofer-Szalkay H, Rössler A, Patwardhan AR,
671 Brown DR, Ziegler MG, Knapp CF.** Centrifuge training increases presyncopal orthostatic
672 tolerance in ambulatory men. *Aviat Sp Environ Med* 75: 850–858, 2004.
- 673 17. **Gibson BYJG, Evans WA.** Clinical studies of the blood volume. II. The relation of plasma and
674 total blood volume to venous pressure, blood velocity rate, physical measurements, age and sex
675 in ninety normal humans. *J Clin Invest* 16: 317–328, 1937.
- 676 18. **Goswami N, Bruner M, Xu D, Bareille MP, Beck A, Hinghofer-Szalkay H, Blaber AP.**

- 677 Short-arm human centrifugation with 0.4g at eye and 0.75g at heart level provides similar
678 cerebrovascular and cardiovascular responses to standing. *Eur J Appl Physiol* 115: 1569–1575,
679 2015.
- 680 19. **Goswami N, Evans J, Schneider S, Von Der Wiesche M, Mulder E, Rössler A, Hinghofer-**
681 **Szalkay H, Blaber AP.** Effects of individualized centrifugation training on orthostatic tolerance
682 in men and women. *PLoS One* 10, 2015.
- 683 20. **Greenleaf JE, Gundo DP, Watenpaugh DE, Mulenburg GM, Mckenzie MA, Looft-Wilson**
684 **R, Hargens AR.** Cycle-Powered Short Radius (1.9 m) Centrifuge: Effect of Exercise Versus
685 Passive Acceleration on Heart Rate in Humans. In: *NASA Technical Memorandum 110433.*
686 Moffett Field, California: 1997, p. 1–14.
- 687 21. **Guyton A, AW L, Kaufmann B.** Effect of Mean Circulatory Filling Pressure and Other
688 Circulatory Factors on Cardiac Output. *Am J Physiol* 180: 463–468, 1955.
- 689 22. **Guyton AC, Coleman TG, Granger HJ.** Circulation: overall regulation. *Annu Rev Physiol* 34:
690 13–46, 1972.
- 691 23. **Guyton AC, Jones CE, Coleman TG.** *Circulatory Physiology: Cardiac Output and Its*
692 *Regulation.* 2nd Ed. Philadelphia: WB Saunders, 1973.
- 693 24. **Heldt T, Mukkamala R, Moody GB, Mark RG.** CVSim: An Open-Source Cardiovascular
694 Simulator for Teaching and Research. *Open Pacing Electrophysiol Ther J* 3: 45–54, 2010.
- 695 25. **Heldt T, Shim EB, Kamm RD, Mark RG.** Computational modeling of cardiovascular response
696 to orthostatic stress. *J Appl Physiol* 92: 1239–1254, 2002.
- 697 26. **van Heusden K, Gisolf J, Stok WJ, Dijkstra S, Karemaker JM.** Mathematical modeling of
698 gravitational effects on the circulation: importance of the time course of venous pooling and
699 blood volume changes in the lungs. *AJP Hear Circ Physiol* 291: H2152–H2165, 2006.
- 700 27. **Iwasaki K-I, Shiozawa T, Kamiya A, Michikami D, Hirayanagi K, Yajima K, Iwase S,**
701 **Mano T.** Hypergravity exercise against bed rest induced changes in cardiac autonomic control.
702 *Eur J Appl Physiol* 94: 285–291, 2005.
- 703 28. **Iwase S.** Effectiveness of centrifuge-induced artificial gravity with ergometric exercise as a
704 countermeasure during simulated microgravity exposure in humans. *Acta Astronaut* 57: 75–80,
705 2005.
- 706 29. **Iwase S, Fu Q, Narita K, Morimoto E, Takada H, Mano T.** Effects of graded load of artificial
707 gravity on cardiovascular functions in humans. *Environ Med* 46: 29–32, 2002.
- 708 30. **Katayama K, Sato K, Akima H.** Acceleration with Exercise during Head-Down Bed Rest
709 Preserves Upright Exercise Responses. *Aviat Sp Environ Med* 75: 1029–1035, 2004.
- 710 31. **Kokalari I, Karaja T, Guerrisi M.** Review on lumped parameter method for modeling the
711 blood flow in systemic arteries. *J Biomed Sci Eng* 6: 92–99, 2013.
- 712 32. **Lau V-K, Sagawa K, Suga H.** Instantaneous pressure-volume relationship of right atrium
713 during isovolumic in canine heart. *Am J Physiol - Hear Circ Physiol* 236: H672–H679, 1979.
- 714 33. **Lee SMC, Feiveson AH, Stein S, Stenger MB, Platts SH.** Orthostatic Intolerance After ISS
715 and Space Shuttle Missions. *Aerosp Med Hum Perform* 86: 54–67, 2015.
- 716 34. **Lim E, Chan GSH, Dokos S, Ng SC, Latif L a, Vandenberghe S, Karunanithi M, Lovell**
717 **NH.** A cardiovascular mathematical model of graded head-up tilt. *PLoS One* 8: e77357, 2013.

- 718 35. **Linnarsson D, Hughson RL, Fraser KS, Clément G, Karlsson LL, Mulder E, Paloski WH,**
719 **Rittweger J, Wuyts FL, Zange J.** Effects of an artificial gravity countermeasure on orthostatic
720 tolerance, blood volumes and aerobic power after short-term bed rest (BR-AG1). *J Appl Physiol*
721 118: 29–35, 2015.
- 722 36. **Melchior FM, Srinivasan RS, Charles JB.** Mathematical modeling of human cardiovascular
723 system for simulation of orthostatic response. *Am J Physiol* 262: H1920–H1933, 1992.
- 724 37. **Melchior FM, Srinivasan RS, Thullier PH, Clère JM.** Simulation of cardiovascular response
725 to lower body negative pressure from 0 to -40 mmHg. *J Appl Physiol* 77: 630–640, 1994.
- 726 38. **Olufsen M, Tran H, Ottesen J.** Modeling cerebral blood flow control during posture change
727 from sitting to standing. *Cardiovasc Eng* 4: 47–58, 2004.
- 728 39. **Olufsen MS, Ottesen JT, Tran HT, Ellwein LM, Lipsitz L a, Novak V.** Blood pressure and
729 blood flow variation during postural change from sitting to standing: model development and
730 validation. *J Appl Physiol* 99: 1523–1537, 2005.
- 731 40. **Ploutz-Snyder LL, Downs M, Goetchius E, Crowell B, English KL, Ploutz-Snyder R, Ryder**
732 **J, Dillon EL, Sheffield-Moore M, Scott JM.** Exercise Training Mitigates Multi-System
733 Deconditioning during Bed Rest. 2018.
- 734 41. **Reisner AT, Heldt T.** A computational model of hemorrhage and dehydration suggests a
735 pathophysiological mechanism: Starling-mediated protein trapping. *AJP Hear Circ Physiol* 304:
736 H620–H631, 2013.
- 737 42. **Sjöstrand T.** Volume and Distribution of Blood and Their Significance in Regulating the
738 Circulation. *Physiol Rev* 33: 202–228, 1953.
- 739 43. **Sprangers RL, Wesseling KH, Imholz AL, Imholz BP, Wieling W.** Initial blood pressure fall
740 on stand up and exercise explained by changes in total peripheral resistance. *J Appl Physiol* 70:
741 523–530, 1991.
- 742 44. **Stenger MB, Evans JM, Knapp CF, Lee SMC, Phillips TR, Perez SA, Moore AD, Paloski**
743 **WH, Platts SH.** Artificial gravity training reduces bed rest-induced cardiovascular
744 deconditioning. *Eur J Appl Physiol* 112: 605–616, 2012.
- 745 45. **Stenger MB, Evans JM, Patwardhan AR, Moore FB, Hinghofer-Szalkay H, Rössler A,**
746 **Ziegler MG, Knapp CF.** Artificial gravity training improves orthostatic tolerance in ambulatory
747 men and women. *Acta Astronaut* 60: 267–272, 2007.
- 748 46. **Taelman L, Degroote J, Verdonck P, Vierendeels J, Segers P.** Modeling hemodynamics in
749 vascular networks using a geometrical multiscale approach: numerical aspects. *Ann Biomed Eng*
750 41: 1445–58, 2013.
- 751 47. **W Leggett R, Williams L.** A Proposed Blood Circulation Model for Reference Man. 1995.
- 752 48. **Wang YC, Yang C Bin, Wu YH, Gao Y, Lu DY, Shi F, Wei XM, Sun XQ.** Artificial gravity
753 with ergometric exercise as a countermeasure against cardiovascular deconditioning during 4
754 days of head-down bed rest in humans. *Eur J Appl Physiol* 111: 2315–2325, 2011.
- 755 49. **Watenpaugh DE.** Fluid volume control during short-term space flight and implications for
756 human performance. *J Exp Biol* 204: 3209–3215, 2001.
- 757 50. **Westerhof N, Lankhaar J-W, Westerhof BE.** The arterial Windkessel. *Med Biol Eng Comput*
758 47: 131–141, 2009.
- 759 51. **Yang C Bin, Zhang S, Zhang Y, Wang B, Yao Y-J, Wang YC, Wu YH, Liang W Bin, Sun**

- 760 **XQ.** Combined short-arm centrifuge and aerobic exercise training improves cardiovascular
761 function and physical working capacity in humans. *Med Sci Monit* 16: 575–583, 2010.
- 762 52. **Yang Y, Baker M, Graf S, Larson J, Caiozzo VJ.** Hypergravity resistance exercise: the use of
763 artificial gravity as potential countermeasure to microgravity. *J Appl Physiol* 103: 1879–87,
764 2007.
- 765 53. **Yang Y, Kaplan A, Pierre M, Adams G, Cavanagh P, Takahashi C, Kreitenberg A, Hicks**
766 **J, Keyak J, Caiozzo V.** Space cycle: a human-powered centrifuge that can be used for
767 hypergravity resistance training. [Online]. *Aviat Sp Environ Med* 78: 2–9, 2007.
768 <http://www.ncbi.nlm.nih.gov/pubmed/17225475>.
- 769 54. **Zamanian SA.** Modeling and Simulating Human Cardiovascular Response to Acceleration. MS
770 Thesis, Massachusetts Institute of Technology: 2007.
- 771 55. **Zhang Q, Evans JM, Stenger MB, Moore FB, Knapp CF.** Autonomic Cardiovascular
772 Responses to Orthostatic Stress After a Short Artificial Gravity Exposure. *Aerosp Med Hum*
773 *Perform* 88: 827–833, 2017.
- 774

775 **FIGURE CAPTIONS**

776

777 **Figure 1.** Circuit representation of the 21-compartment cardiovascular model, composed of 4 sections:
778 head and arms, thorax, abdomen, and legs. Systemic compartments include proximal aorta (1),
779 brachiocephalic arteries (2), upper body precapillary (3) and postcapillary (4) compartments, superior
780 vena cava (5), thoracic aorta (6), abdominal aorta (7), renal precapillary (8) and postcapillary (9)
781 compartments, splanchnic precapillary (10) and postcapillary (11) compartments, leg precapillary (12)
782 and postcapillary (13) compartments, abdominal veins (14), and thoracic inferior vena cava (15). Four
783 microvascular resistances are also included: upper body R_{ub} , kidneys R_{rc} , splanchnic R_{sc} , and legs R_{lc} .
784 The right heart and left heart include variable capacitors and diodes representing the heart valves that
785 prevent reversal flow. The pulmonary circulation is represented by two compartments (pre and post
786 capillary components) connected by a microvascular resistor. Two vein compartments (Compartments
787 4–upper body and 13–leg) also include diodes to capture the unidirectional nature of the venous flow
788 due to the presence of venous valves.

789 **Figure 2.** Single representation of the n^{th} compartment, where R_n is the resistance, C_n is the
790 (incremental) vascular compliance (C_n is defined as $dV_n/d\Delta P_n$), P_n is the compartment pressure, q_n
791 is the flow rate; $P_{h,n}$ is the hydrostatic pressure; and $P_{ext,n}$ is the external pressure (e.g. intra-thoracic
792 pressure, intra-abdominal pressure, muscle pump pressure). The arrows over the compliance
793 (represented by the electric symbol of a capacitor) and pressure sources (represented by open circles)
794 indicate the variable nature of these elements, either as a function of filling status (capacitors) or as a
795 function of time (pressure sources).

796 **Figure 3.** Exercise protocol conducted by twelve subjects on the MIT short-radius centrifuge. The
797 protocol consisted of the following phases: baseline (3 min), spin-up phase to the desired G-level (~100
798 sec), AG phase with only centrifugation (~2min), AG & Exercise phase (15 min), AG phase with no
799 exercise for subjects to partially recover (2 min), and spin-down phase (1 min). We simulated an
800 identical profile with our computational model and used the experimental data for validation purposes.
801 Figure adapted from (10).

802 **Figure 4.** Simulated (black line) and experimental (grey line, mean \pm SD including 12 subjects)
803 cardiovascular responses to centrifugation at 1G (measured at the feet) and ergometer exercise in a
804 short-radius centrifuge.

805 **Figure 5.** Simulated (black line) and experimental (grey line, mean \pm SD including 12 subjects)
806 cardiovascular responses to centrifugation at 1.4G (measured at the feet) and ergometer exercise in a
807 short-radius centrifuge.

808 **Figure 6.** Simulated cardiovascular responses to centrifugation at 1G (measured at the feet) and
809 ergometer exercise varying blood volume conditions. Data are reported for all protocol phases: baseline
810 (BL), centrifugation alone (AG), and centrifugation combined with exercise (25W, 50W, and 100W).
811 Blood volume levels include baseline blood volume ($V_{\text{total}} = 5175 \text{ ml}$) and blood volume reductions
812 of 5%, 10%, and 15%.

813

814 **TABLES**

815

816 **Table 1:** Mathematical expressions capturing orthostatic stress during short-radius centrifugation
 817 through three mechanisms: 1) changes in hydrostatic pressure (term included in all systemic
 818 compartments), 2) changes in intrathoracic pressure (due to the weight of the liver being pulled down in
 819 the thoracic compartment; term included in compartments within the thorax region), and 3) changes in
 820 total blood volume (due to the increase in transcapillary fluid flow into the dependent vasculature)

Gravitational Effect	Short-radius Centrifugation
Hydrostatic pressure	$P_{h,n} = \frac{1}{2} \rho \omega^2(t) (R_{0,n}^2 - R_{i,n}^2)$
Intrathoracic pressure	$P_{th}(t) = P_{th_0} - 3.5 \frac{(r + d)^2 \cdot \omega_{max}^2}{g^2} \cdot \omega^2(t)$
Maximum Interstitial Volume Change	$V_{max} = 300ml \cdot \frac{(r + d) \cdot \omega_{max}^2}{g \cdot \sin(85^\circ)}$

821

822 where $P_{h,n}(t)$ is the hydrostatic pressure, ρ is the density of the blood, $\omega(t)$ is the angular velocity of the
 823 centrifuge, $P_{th}(t)$ is the intrathoracic pressure, P_{th_0} is the nominal intrathoracic pressure without orthostatic stress
 824 (-4 mmHg), ω_{max} is the maximum and final angular velocity achieved, $r = 55 \text{ cm}$ is the distance of the thoracic
 825 compartment to the center of rotation of the centrifuge, d is the distance from the head of the subject to the center
 826 of rotation of the centrifuge ($d = 0 \text{ cm}$), V_{max} is the maximum interstitial volume change (from intravascular
 827 volume to the interstitial space), $R_{i,n}$ is the inner radius of the compartment under consideration (the distance
 828 between the superior end of the compartment and the center of rotation), and $R_{0,n}$ is the outer radius of the
 829 compartment under consideration, which is defined as the sum of the effective length of the compartment and the
 830 inner radius. Note: The effective length of each compartment is defined as one half of its anatomical vertical
 831 length $l_{v,n}$, except for the leg compartments, where the effective length is assumed to be one third of the
 832 anatomical vertical length.

833

834 **Table 2:** Exercise parameters during the different phases of the “1G” and “1.4G” simulations.
 835 Manipulated parameters include P_A^{sp} : set-point reference pressure for the arterial baroreceptor control
 836 system (mmHg); R_{lc} : leg microvascular resistance (Peripheral Resistance Units (PRU) or
 837 mmHg/ml/min.); P_{max}^{pump} : maximal leg external pressure (mmHg); and P_{max}^{abd} : maximal intra-abdominal
 838 pressure (mmHg). P_A^{sp} and P_{max}^{pump} were adjusted to match the experimental Mean Arterial Pressure
 839 (MAP) data, and R_{lc} was adjusted to match the experimental total peripheral resistance (TPR) data.
 840 P_{max}^{abd} was adjusted based on the literature.

841

Simulation phase	Arterial set-point P_A^{sp} (mmHg)		Leg Arterial Resistance R_{lc} (PRU)		Leg external pressure P_{max}^{pump} due to muscle pump (mmHg)		Intra-abdominal pressure P_{max}^{abd} (mmHg)	
	1G	1.4G	1G	1.4G	1G	1.4G	1G	1.4G
AG level (measured at the feet)	1G	1.4G	1G	1.4G	1G	1.4G	1G	1.4G
Baseline	93	93	3.9	3.9	0	0	2	2
AG after Spin-up	93	93	3.9	3.9	20**	30**	2	2
Exercise: 25W	120	125	1.15*	1*	40***	65***	2.5	2.5
Exercise: 50W	135	140	0.75*	0.75*	50***	75***	6	6
Exercise: 100W	205	225	0.54*	0.54*	60***	90***	10	10
AG before Spin-down	105	105	2.4*	2.4*	20**	30**		
Rest	105	105			0	0		

842 * resistance disconnected from controls

843 ** constant

844 *** periodic 1 sec

845

846

847

848

849

850 **Table 3:** Simulated (Sim) and experimental (Exp, values are mean \pm SD) average of cardiovascular variables during the different phases of the
 851 protocol at the two G-levels investigated: 1G and 1.4G (measured at the feet). For both simulated and experimental data, averages were calculated
 852 including the last 2 minutes of each period.

853
 854

CV Variable	Baseline				AG				AG +Exercise 25W				AG + Exercise 50W				AG + Exercise 100W			
	1G		1.4G		1G		1.4G		1G		1.4G		1G		1.4G		1G		1.4G	
	Sim	Exp	Sim	Exp	Sim	Exp	Sim	Exp	Sim	Exp	Sim	Exp	Sim	Exp	Sim	Exp	Sim	Exp	Sim	Exp
CO (l/min)	5.9	6.1 \pm 1.2	5.9	6.5 \pm 1.1	5.8	5.8 \pm 1.3	6.0	6.7 \pm 1.3	8.7	9.5 \pm 2.2	9.8	10.9 \pm 1.5	10.6	12.1 \pm 2.3	11.6	13.2 \pm 2.3	13.2	15.8 \pm 2.8	14.5	16.7 \pm 2.5
SV (ml)	87.9	96.2 \pm 14.0	87.9	101.0 \pm 11.9	83.2	91.0 \pm 15.4	84.5	98.2 \pm 14.3	90.0	98.8 \pm 20.8	97.7	107.9 \pm 14.1	96.7	110.5 \pm 19.2	104.6	115.5 \pm 17.8	98.5	114.8 \pm 17.4	106.4	120.3 \pm 20.3
HR (bpm)	67.3	64.1 \pm 9.0	67.3	64.9 \pm 10.0	67.7	64.5 \pm 9.2	67.7	69.3 \pm 11.9	96.2	97.0 \pm 10.5	100.0	101.6 \pm 12.8	109.3	110.3 \pm 12.4	110.6	114.4 \pm 14.2	133.7	138.1 \pm 17.6	136.3	140.2 \pm 17.4
SBP (mmHg)	116.9	116.6 \pm 6.5	116.9	123.4 \pm 9.7	115.4	116.5 \pm 11.6	116.4	121.7 \pm 11.9	124.3	128.1 \pm 13.6	128.6	136.6 \pm 11.5	129.3	138.1 \pm 14.2	135.3	151.0 \pm 16.7	140.4	151.0 \pm 17.5	147.5	158.7 \pm 19.9
MBP (mmHg)	92.9	90.4 \pm 4.9	92.9	94.4 \pm 7.4	92.8	90.5 \pm 8.3	93.5	92.8 \pm 9.7	100.8	98.6 \pm 10.3	103.2	103.2 \pm 11.1	104.1	101.8 \pm 10.6	108.3	108.1 \pm 10.4	115.0	110.7 \pm 12.9	120.3	113.8 \pm 14.7
DBP (mmHg)	67.8	73.2 \pm 4.3	67.8	75.8 \pm 6.7	68.9	74.2 \pm 6.9	69.2	74.5 \pm 8.8	74.9	80.0 \pm 8.6	75.1	81.7 \pm 9.2	76.4	80.7 \pm 7.4	78.4	84.7 \pm 7.7	86.6	86.0 \pm 9.8	89.7	87.2 \pm 11.2
PP (mmHg)	49.1	43.4 \pm 6.8	49.1	47.6 \pm 5.8	46.5	42.4 \pm 9.1	47.2	47.2 \pm 7.6	49.5	48.2 \pm 10.6	53.5	54.9 \pm 6.3	52.8	57.4 \pm 9.7	57.0	66.3 \pm 11.1	53.7	65.0 \pm 10.2	57.8	71.5 \pm 10.3
TPR (PRU)	0.86	0.93 \pm 0.2	0.86	0.90 \pm 0.2	0.86	0.98 \pm 0.3	0.86	0.86 \pm 0.2	0.62	0.66 \pm 0.2	0.58	0.59 \pm 0.1	0.49	0.53 \pm 0.1	0.49	0.52 \pm 0.1	0.40	0.44 \pm 0.1	0.40	0.44 \pm 0.1

855
 856
 857

858 **Table 4:** Values of the cardiovascular model parameters

859

Resistance (PRU)	Unstressed volume (mL)	Compliance (mL/mm Hg)	Anatomical vertical length (cm)	Elastances Cardiac Model (mm Hg/mL)	Regulatory Control Systems	Additional Parameters
$R_1=0.007$	$V_{0,1}=21$	$C_1=0.28$	$l_{v,1}=10.0$	$E_{es,ra}=0.74$	$P_A^{sp}=93$ mm Hg	$P_{th0}=-4$ mm Hg
$R_2=0.003$	$V_{0,2}=5$	$C_2=0.13$	$l_{v,2}=4.5$	$E_{d,ra}=0.3$	$G_{R-R}^{A,S}=9$	$V_{tot}=5175$ mL
$R_3=0.014$	$V_{0,3}=200$	$C_3=0.2$	$l_{v,3}=20.0$	$E_{es,rv}=1.3$	$G_{R-R}^{A,P}=9$	$HR_{nom}=67$ beats/min
$R_4=0.11$	$V_{0,4}=645$	$C_4=7.0$	$l_{v,4}=20.0$	$E_{d,rv}=0.05$	$G_{C_{lv}}^{A,S}=0.007$	$BW=69$ Kg
$R_5=0.028$	$V_{0,5}=16$	$C_5=1.3$	$l_{v,5}=14.5$	$E_{es,la}=0.61$	$G_{C_{rv}}^{A,S}=0.022$	
$R_6=0.011$	$V_{0,6}=16$	$C_6=0.1$	$l_{v,6}=16.0$	$E_{d,la}=0.5$	$G_{R_{ub}}^{A,S}=-0.05$	
$R_7=0.010$	$V_{0,7}=10$	$C_7=0.1$	$l_{v,7}=14.5$	$E_{es,lv}=2.5$	$G_{R_{rc}}^{A,S}=-0.05$	
$R_8=0.10$	$V_{0,8}=20$	$C_8=0.21$	$l_{v,8}=0$	$E_{d,lv}=0.11$	$G_{R_{sc}}^{A,S}=-0.05$	
$R_9=0.11$	$V_{0,9}=30$	$C_9=5.0$	$l_{v,9}=0$		$G_{R_{lc}}^{A,S}=-0.05$	
$R_{10}=0.07$	$V_{0,10}=300$	$C_{10}=0.2$	$l_{v,10}=10.0$		$G_{V_{ub}}^{A,S}=5$	
$R_{11}=0.07$	$V_{0,11}=1146$	$C_{11}=50$	$l_{v,11}=10.0$		$G_{V_{rc}}^{A,S}=2$	
$R_{12}=0.09$	$V_{0,12}=200$	$C_{12}=0.2$	$l_{v,12}=85$		$G_{V_{sc}}^{A,S}=13$	
$R_{13}=0.10$	$V_{0,13}=716$	$C_{13}=20$	$l_{v,13}=85$		$G_{V_{lc}}^{A,S}=7$	
$R_{14}=0.019$	$V_{0,14}=79$	$C_{14}=1.3$	$l_{v,14}=14.5$		$P_{CP}^{sp}=6$ mm Hg	
$R_{15}=0.008$	$V_{0,15}=33$	$C_{15}=0.5$	$l_{v,15}=6$		$G_{R_{ub}}^{CP,S}=-0.05$	
$R_{tri}=0.006$	$V_{0,ra}=14$	$C_{pa}=3.4$			$G_{R_{rc}}^{CP,S}=-0.05$	
$R_{pa}=0.006$	$V_{0,rv}=46$	$C_{pv}=9.0$			$G_{R_{sc}}^{CP,S}=-0.05$	
$R_{pc}=0.07$	$V_{0,pa}=160$				$G_{R_{lc}}^{CP,S}=-0.05$	
$R_{pv}=0.006$	$V_{0,pv}=430$				$G_{V_{ub}}^{CP,S}=13$	
$R_{mit}=0.010$	$V_{0,la}=24$				$G_{V_{rc}}^{CP,S}=3$	
$R_{ub}=4.0$	$V_{0,lv}=55$				$G_{V_{sc}}^{CP,S}=64$	
$R_{rc}=4.2$					$G_{V_{lc}}^{CP,S}=30$	
$R_{sc}=2.4$						
$R_{lc}=3.9$						

860 R : resistances; V_0 : unstressed volumes; C : compliances; l_v : anatomical vertical lengths; E : elastances; P :
 861 pressures; G : gains factors; V : volumes; HR : heart rate; BW : body weight. Abbreviations: ra, right atrium; tri,
 862 tricuspid valve; rv, right ventricle; pa, pulmonary arteries; pc, pulmonary circulation; pv, pulmonary veins; la, left
 863 atrium; mit, mitral valve; lv, left ventricle; ub, upper body; rc, renal circulation, sc, splanchnic circulation; lc, leg
 864 circulation; es, end-systolic elastance; d, diastolic elastance; A, arterial baroreflex; CP, cardiopulmonary reflex; sp,
 865 set-point; S, sympathetic, P, parasympathetic; R-R, R-R interval; th_0 , nominal intra-thoracic.

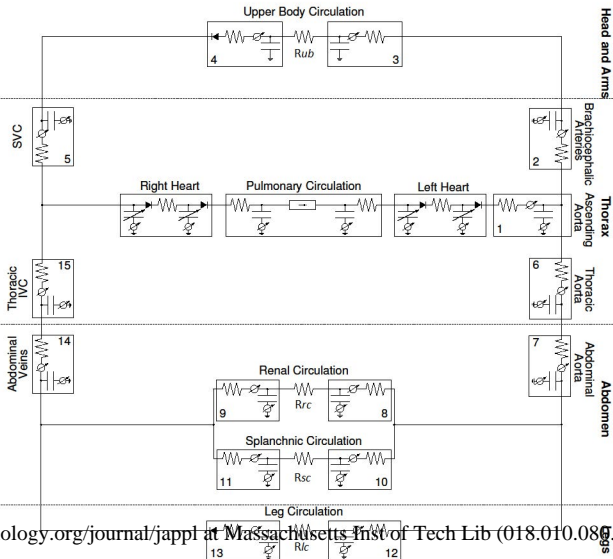
866

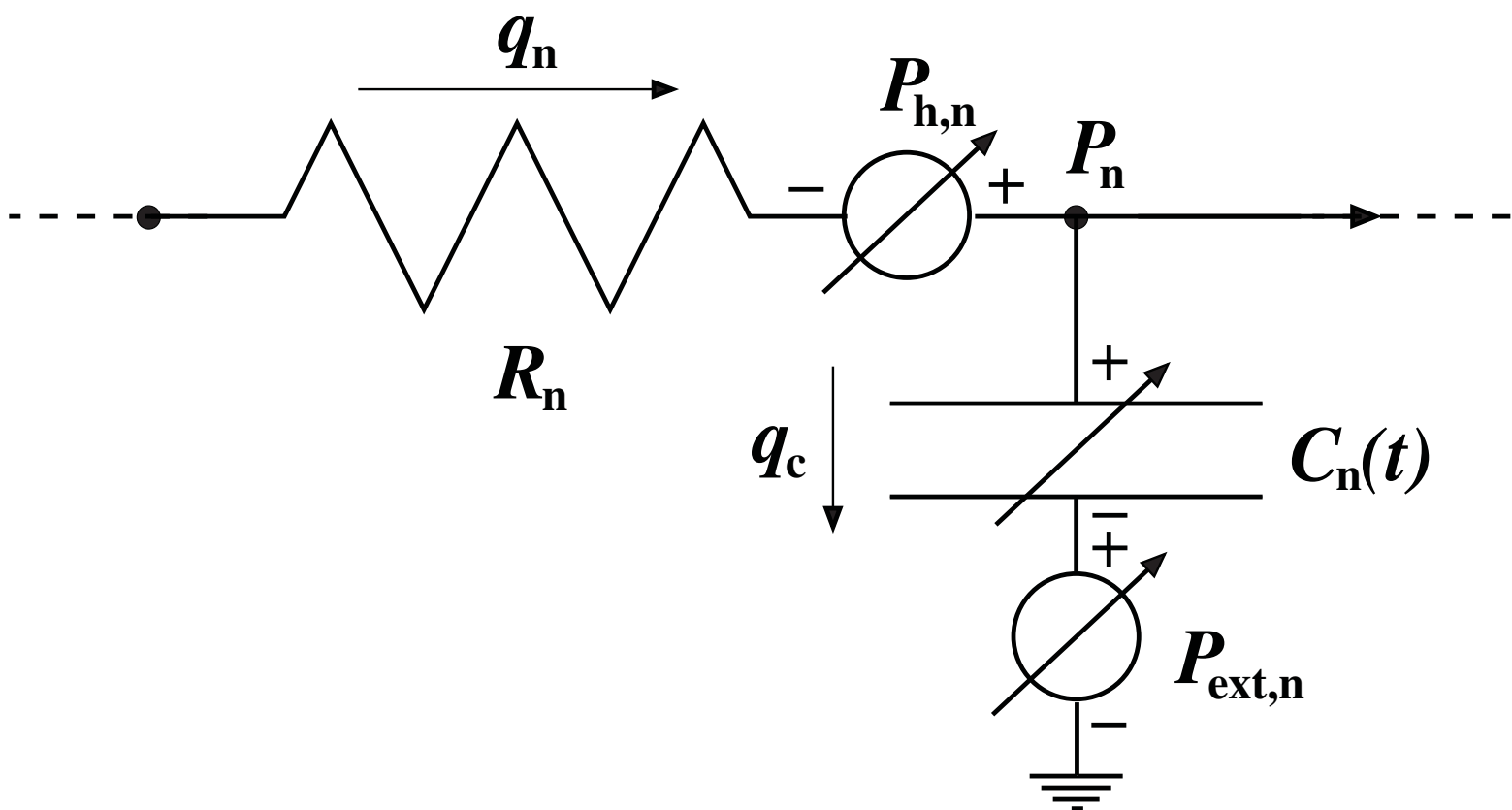
867

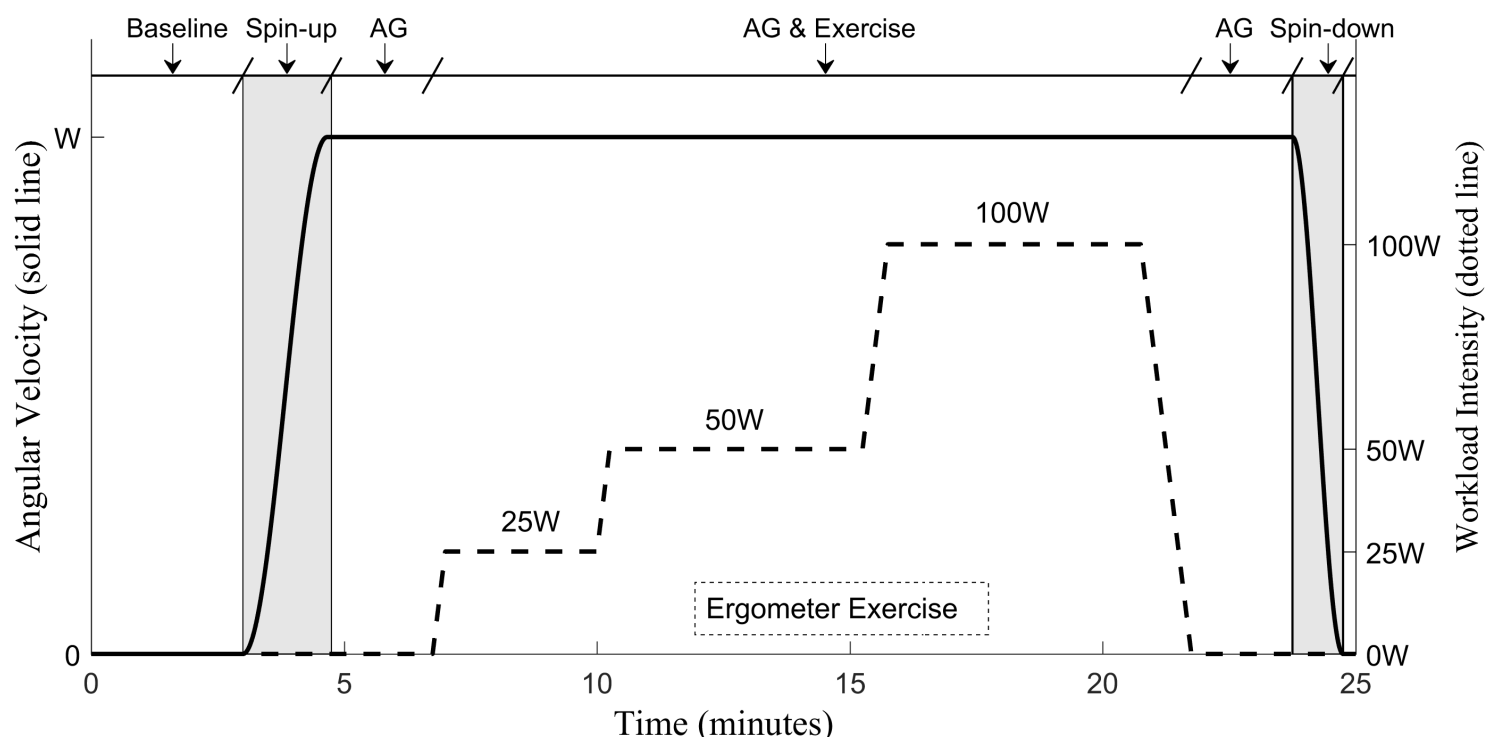
868 **Table 5:** Flow and Volume parameters in each of the compartments during steady-state simulation in
 869 supine position.

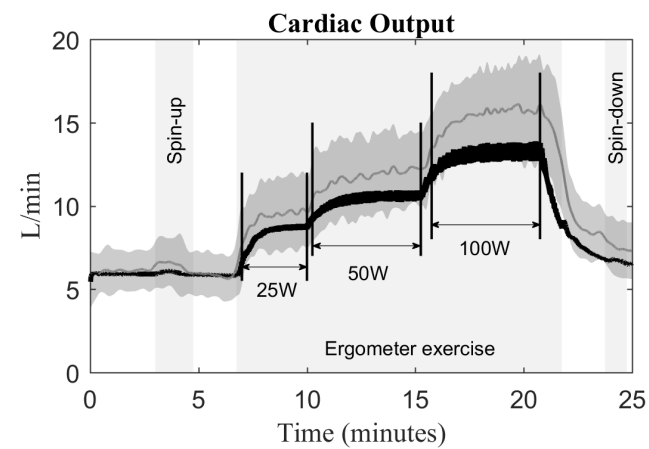
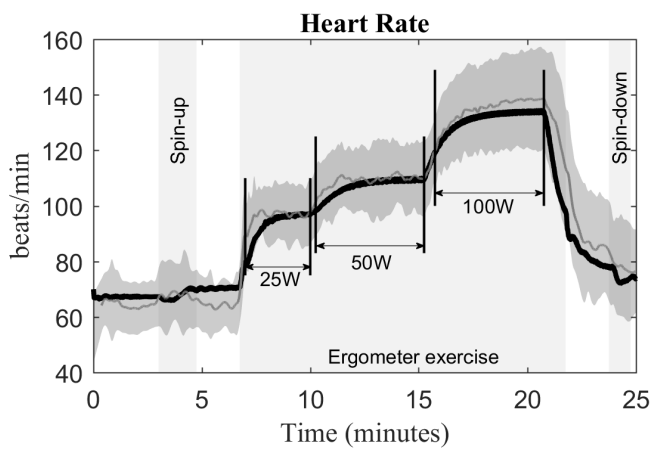
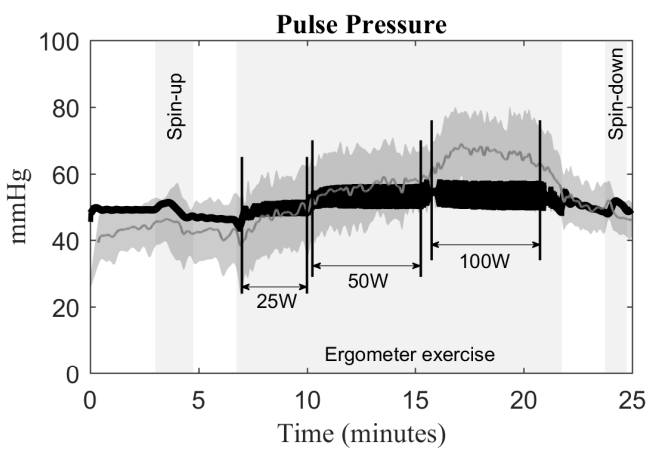
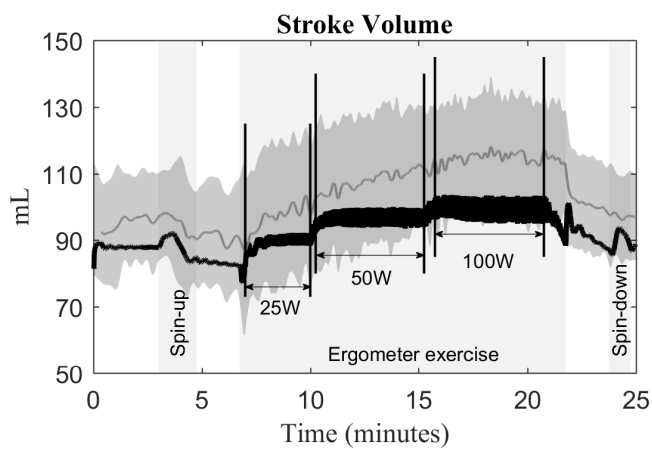
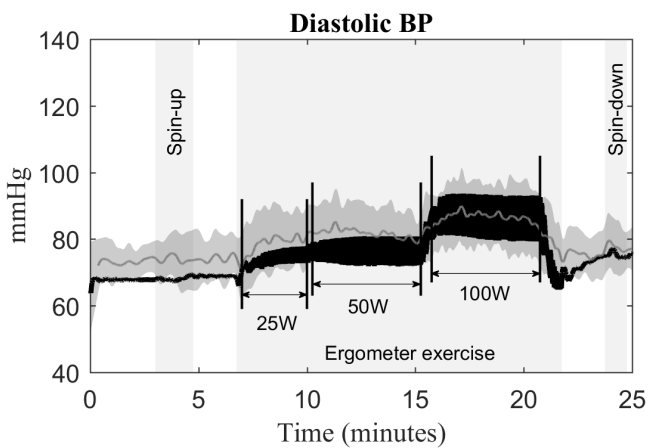
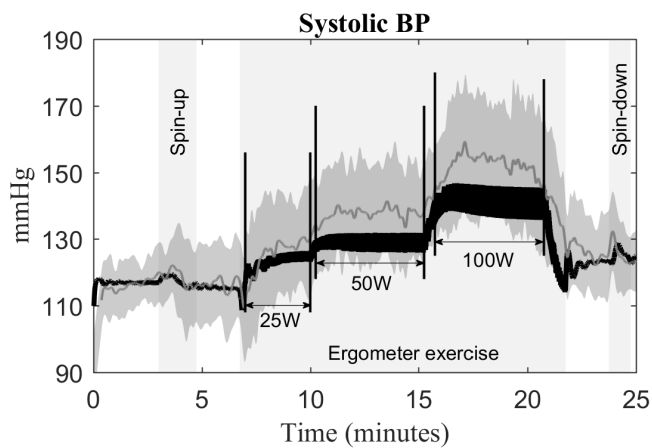
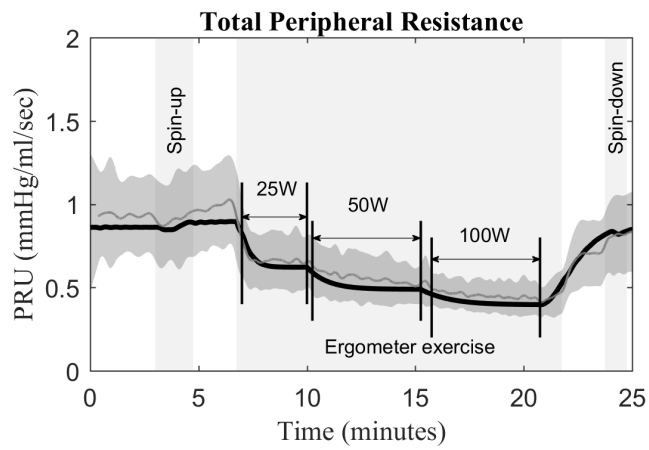
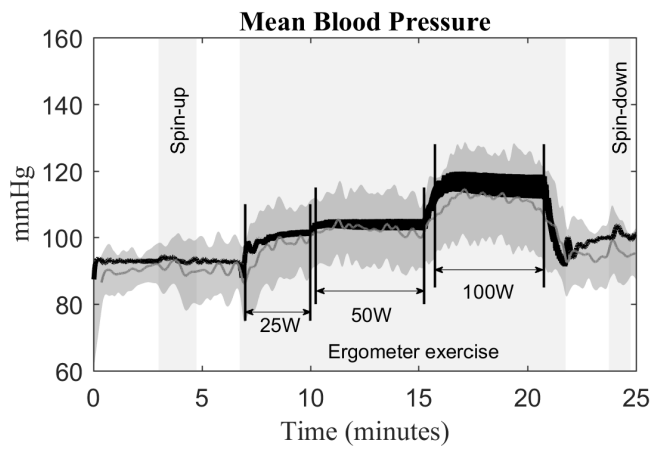
Upper Body Circulation		Heart Circulation		Thoracic and Abdominal Circulation		Splanchnic Circulation		Renal Circulation		Leg Circulation	
Flow (l/min)	Volume (ml)	Flow (l/min)	Volume (ml)	Flow (l/min)	Volume (ml)	Flow (l/min)	Volume (ml)	Flow (l/min)	Volume (ml)	Flow (l/min)	Volume (ml)
$Q_{2i} = 1.34$	$V_2 = 17.6$	$Q_{rai} = 5.85$	$V_{ra} = 31.8$	$Q_{6i} = 4.56$	$V_6 = 25.6$	$Q_{10i} = 2.07$	$V_{10} = 317.8$	$Q_{8i} = 1.19$	$V_8 = 38.8$	$Q_{12i} = 1.29$	$V_{12} = 217.9$
$Q_{3i} = 1.33$	$V_3 = 218.5$	$Q_{rvi} = 5.86$	$V_{rv} = 110.5$	$Q_{7i} = 4.55$	$V_7 = 19.1$	$Q_{11i} = 2.06$	$V_{11} = 1382.7$	$Q_{9i} = 1.18$	$V_9 = 52.2$	$Q_{13i} = 1.28$	$V_{13} = 845.9$
$Q_{4i} = 1.31$	$V_4 = 682.9$	$Q_{rvo} = 5.88$	$V_{la} = 54.5$	$Q_{14i} = 4.52$	$V_{14} = 81.9$	$Q_{11o} = 2.06$		$Q_{9o} = 1.19$		$Q_{13o} = 1.28$	
$Q_{5i} = 1.31$	$V_5 = 24.8$	$Q_{pc} = 5.85$	$V_{lv} = 153.8$	$Q_{15i} = 4.53$	$V_{15} = 36.4$						
$Q_{5o} = 1.32$		$Q_{lai} = 5.91$	$V_1 = 48.1$	$Q_{15o} = 4.53$							
		$Q_{lvi} = 5.92$									
		$Q_{lvo} = 5.91$									

870 Q_{ni} , flow going into the compartment n ; Q_{no} , flow going out the compartment n ; ra, right atrium; rv, right
 871 ventricle; la, left atrium; lv, left ventricle;

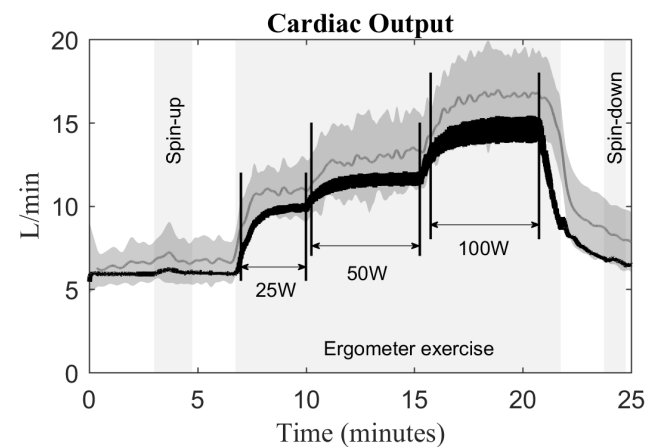
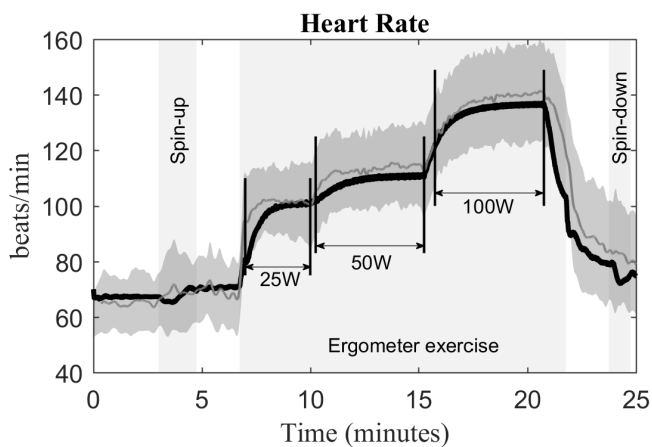
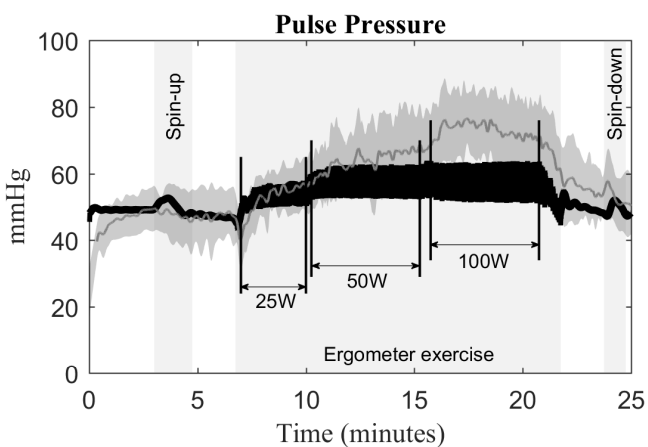
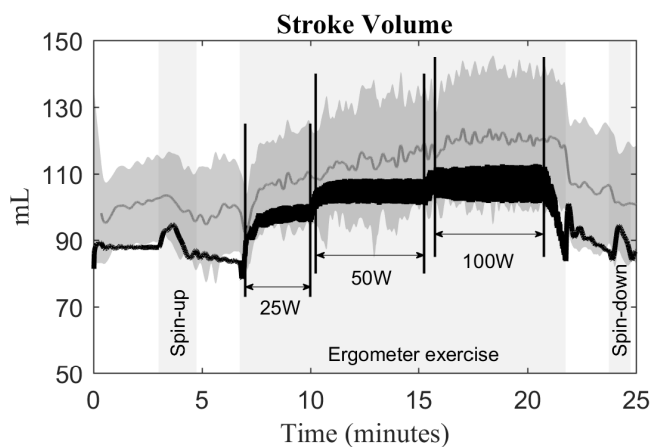
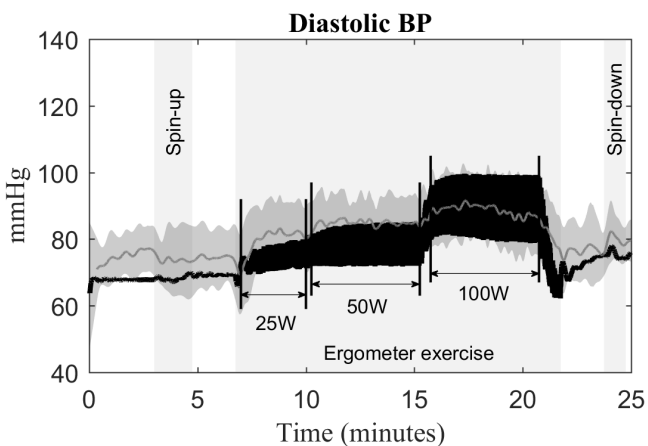
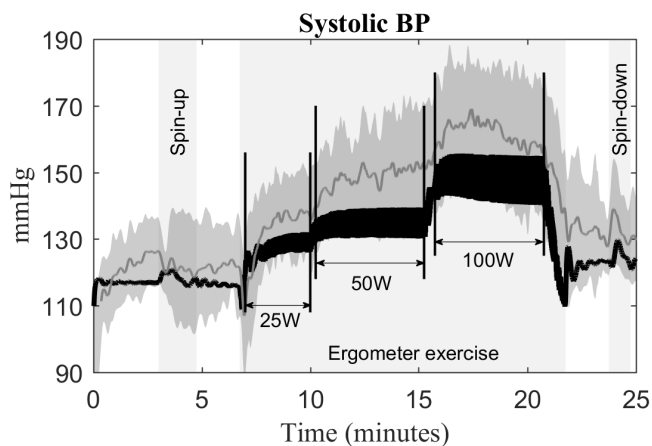
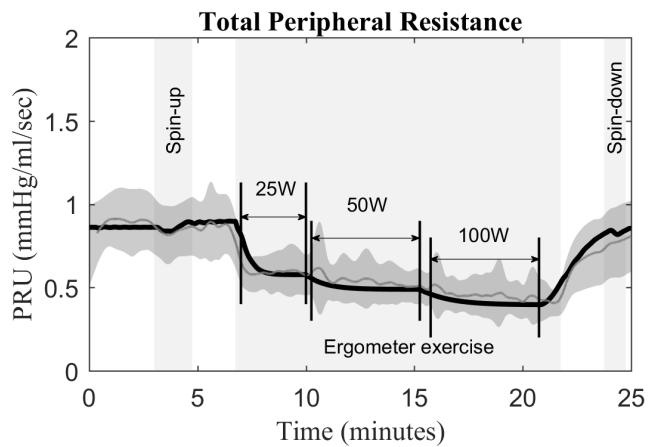
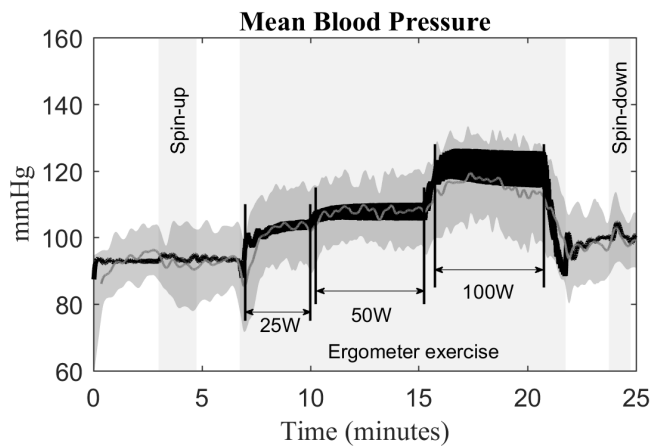








— Computational model prediction at 1G — Experimental data (mean ± SD) at 1G



— Computational model prediction at 1.4G — Experimental data (mean ± SD) at 1.4G

